NASA CONTRACTOR REPORT

NASA CR-6

NASA CR-600
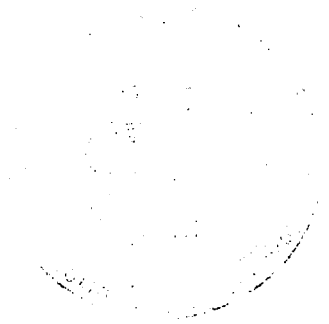
AN ANALYTICAL STUDY OF SEPARATED FLOWS INDUCED BY SHOCK WAVE - BOUNDARY LAYER INTERACTION

by M. S. Holden

Prepared by
CORNELL AERONAUTICAL LABORATORY, INC.
Buffalo, N. Y.
for Goddard Space Flight Center

NATIONAL AERONAUTICS AND SPACE ADMINISTRATION • WASHINGTON, D. C. • OCTOBER 1966

NASA CR-600

AN ANALYTICAL STUDY OF SEPARATED FLOWS INDUCED BY

SHOCK WAVE - BOUNDARY LAYER INTERACTION

By M. S. Holden

Distribution of this report is provided in the interest of information exchange. Responsibility for the contents resides in the author or organization that prepared it.

FOREWORD

The work described in this report was supported by the National Aeronautics and Space Administration, Goddard Space Center under Contract NAS 5-3976.

The author wishes to acknowledge the assistance of Mr. Harold Rosenbaum of the Computer Services Department in carrying out the computer solutions discussed in this report.

ABSTRACT

This report presents an analysis of laminar regions of shock wave - boundary layer interaction in highly cooled supersonic and hypersonic flows. In this analysis the integral forms of the boundary layer equations are used to describe the development of the viscous layer and its interaction with the outer inviscid flow. The boundary layer equations governing conservation of mass, momentum, moment of momentum, and energy are solved simultaneously by numerical integration to yield a continuous solution over the entire interaction. The parameters required to define the properties of a specific interaction are the wall-to-stagnation temperature ratio, the Mach number of the free stream, the free-stream Reynolds number based on the length of the flat plate or the distance to shock impingement, and the Mach number downstream of the interaction (as defined by inviscid flow considerations). This method enables the detailed distribution of pressure, skin friction, and heat transfer to the walls bounding the interaction to be calculated. Further, the method describes the form and detailed development of the velocity and enthalpy profiles throughout the interaction region.

The theory has been applied to calculate both wedge- and shock-induced interactions for comparison with previously published experimental data for a Mach 6 airflow over an adiabatic wall and a Mach 10 airflow over a highly cooled wall. The theory is in good agreement with experimental surface pressure and heat transfer distributions through shock-induced separated regions over a highly cooled wall in a Mach 10

airflow obtained by Holden. For the limiting case of an adiabatic wall, the present solutions for the Mach 6 flow are in excellent agreement with a theory proposed earlier by Lees and Reeves, and with the experimental pressure data of Sterret and Emery.

A study has been made, using this theory, of the way in which the properties of an interaction change when the strength of the adverse pressure gradient inducing the interaction is varied. The theory has also been applied to calculate the incipient separation conditions for a laminar boundary layer.

TABLE OF CONTENTS

NOMENCLATURE

a velocity profile parameter   (i) $\left[\partial(U/U_e)/\partial(Y/\delta_i)\right]_w$

for attached flows

(ii) $\left[Y/\delta_i\right]_{U/U_e = 0}$

for separated flows

a   speed of sound

b   enthalpy profile parameters $\left[-\dfrac{\partial}{\partial Y}\left(\dfrac{s}{s_w}\right)\right]_w$ for both attached or separated flows

c   coefficients on the power series or the profile parameters

C $\left[H + \left(\dfrac{m_e + 1}{m_e}\right)\left(1 + s_w\, t\right)\right]$

c_v, c_p specific heat at constant volume and constant pressure, respectively

c_F skin friction coefficient $\left(\tau/\tfrac{1}{2}\rho_\infty U_\infty^2\right)$

F $\left[2H + \left(\dfrac{3\gamma - 1}{\gamma - 1}\right) + \left(\dfrac{\gamma + 1}{\gamma - 1}\right)\dfrac{m_e}{1 + m_e}\, H + \left(\dfrac{3\gamma - 1}{\gamma - 1}\right) s_w t + \right.$

$\left. \dfrac{M_e^2 - 1}{m_e(1 + m_e)}\ \dfrac{1}{\delta_i^*}\ \int_0^{\delta_i}\dfrac{U}{U_e}\, dY\right]$

g $-Re_{\delta_{i_o}}\ \delta_R\left(\dfrac{M_e}{M_\infty}\right)\ \dfrac{(1 + m_e)}{m_e(1 + m_\infty)}\ \tan\theta$

h   static enthalpy

h_s total enthalpy

H θ_i/δ_i^*

I $\displaystyle\int_0^{\delta_i} s/s_w\ dY$

J θ_i^*/δ_i^*

K $\displaystyle\int_0^{\delta_i}\dfrac{s}{s_w}\ \dfrac{U}{U_e}\ dY$

m $\left(\dfrac{\gamma - 1}{2}\right)M^2$

M — Mach number

$M_{1,2,3,4}$ — functions defined in Eqs. (3.13)-(3.16)

$N_{1,2,3}$ — functions defined in Eqs. (4.1)-(4.3)

p — pressure

P — $(\delta_i/u_e)\left(\dfrac{dU}{dY}\right)_{Y=0}$

Pr — Prandtl number

Q — $\dfrac{d}{dY}\left(\dfrac{s}{s_w}\right)_{Y=0}\delta_i^*$

R — dissipation function $\left(\dfrac{2\delta_i^*}{u_e^2}\right)\displaystyle\int_0^{\delta_i}\left(\dfrac{\partial U}{\partial Y}\right)^2 dY$

Re — Reynolds number

Re_{x_o} — $\left[\dfrac{u_\infty x_o}{\nu_\infty}\right]$

$Re_{\delta_i^*}$ — $\left[\dfrac{u_e \delta_i^*}{\nu_e}\right]$

$\tilde{R}_{\delta_i^*}$ — $\left[\dfrac{a_\infty M_e \delta_i^*}{\nu_\infty}\right]$

S — enthalpy function $\left(\dfrac{h_s}{h_{se}} - 1\right)$

t — I/δ_i^*

T — K/δ_i^*

u — velocity component paralleled to the surface

U — transformed (Stewartson's) velocity, $u\left(\dfrac{a_\infty}{a_e}\right)$

v — velocity component normal to the surface

V — transformed (Stewartson's) velocity

W — $\dfrac{1}{\delta_i^*}\displaystyle\int_0^{\delta_i}\dfrac{U}{U_e}\,dY$

x, y   coordinates parallel to and normal to the surface, respectively

X, Y   Stewartson's transformed coordinates

Y^* distance to the zero velocity streamline in separated flow

α angle of wedge or shock generator

β Falkner-Skan's pressure gradient parameters

γ specific heat ratio, c_p/c_v

δ boundary layer thickness

δ_i transformed boundary layer thickness

δ^* displacement thickness

δ_i^* transformed displacement thickness

δ_R $\delta_i^*/\delta_{i_o}^*$

δ_t^{**} $\delta_i^* + I$

η $Y\sqrt{\left(\dfrac{m+I}{2}\right)\left(\dfrac{u_e}{\nu_\infty X}\right)}$

θ boundary layer momentum thickness

θ^* kinetic energy thickness

Θ local angle between x axis and the streamline at the edge of the boundary layer

λ Pohlhausen parameter

μ dynamic viscosity

ν kinematic viscosity

$\bar{\nu}$ Prandtl-Meyer angle

ρ gas density

$\bar{\tau}$ $s_w\left(\dfrac{I+m_e}{m_e}\right)\left(\dfrac{dt}{dT}\right)$

τ shear stress

ψ stream function

NOMENCLATURE (Cont.)

Subscripts

e	local condition in the inviscid flow just outside the boundary layer
i	incompressible plane
o	condition at the beginning of the interaction
r	reattachment point
s	stagnation conditions
∞_- , ∞	conditions well upstream of the interaction
∞_+	conditions well downstream of the interaction
w	conditions evaluated at the wall

LIST OF TABLES AND FIGURES

I. INTRODUCTION

The interaction between the growth of a boundary layer and the local inviscid stream may significantly modify the performance of compression surfaces such as flaps, flared junctions and intakes on hypersonic re-entry vehicles designed on the basis of inviscid flow calculations. In supersonic and hypersonic flows, laminar regions of shock wave - boundary layer interaction of significant proportions can be created by relatively small adverse pressure gradients. The strength of such interaction is often sufficient to cause boundary-layer separation, thus creating a region of shock-induced separated flow which markedly distorts the distribution of pressure, skin friction, and heat transfer on the compression surface. The occurrence of laminar attached and separated viscous regions in hypersonic flows over a large range of Reynolds numbers makes the analysis of these regions of considerable practical importance.

This paper presents a theoretical analysis of laminar shock wave - boundary layer interaction in highly cooled hypersonic flows. The type of flows studied are those which have been induced by the "free" interaction between a viscous layer and an outer inviscid hypersonic flow. Two general situations are considered in which such flows are generated. The first situation is the flow over a body-flap junction, termed wedge-induced interaction, where the adverse pressure gradient propagating upstream through the subsonic portion of the boundary layer causes boundary layer thickening and interaction with the outer inviscid flow. The second situation, termed shock-induced interaction, is caused by an oblique shock impinging on a

1

boundary layer. The present analysis encompasses both attached and separated flows produced in these situations.

Despite the relative simplicity of the laminar flow model, the complexity of the flow mechanism in such separated regions makes any rational analysis a formidable task. The problem is one of adequately describing the development of the flow in the attached and separated viscous layers, including the interaction between the viscous region and the external inviscid stream.

In the present analysis, the integral forms of the laminar boundary-layer equations are used to describe the development of the viscous layer and its interaction with the outer inviscid stream. The velocity and enthalpy profiles in the highly cooled attached and separated regions are represented by the upper and lower branch solutions, respectively, of the compressible flow analog to the Falkner-Skan equations. The boundary-layer equations governing conservation of mass, momentum, moment of momentum, and energy are used to describe the viscous flow. Expressing the basic partial differential equations in their integral form reduces the problem to the solution of four ordinary, nonlinear differential equations. These equations are solved simultaneously by numerical integration on a digital computer to yield a continuous solution over the entire interaction region. The input parameters required to define the properties of a specific interaction are the wall-to-stagnation temperature ratio, the Mach number of the free stream, the free-stream Reynolds number based on distance to hinge line or shock impingement, and the Mach number downstream of the interaction (as defined by inviscid flow considerations).

The analysis describes both wedge- and shock-induced interactions. This method enables the distribution of pressure, skin friction, and heat transfer to the walls bounding the interaction to be calculated. Further, the method describes the form and detailed development of the velocity and enthalpy profiles throughout the interaction region.

The present theory has been applied to calculate both wedge- and shock-induced interactions for comparison with previously published experimental data for both adiabatic wall and highly cooled wall cases. For the limiting case of shock-induced separated flows over an adiabatic wall, the energy equation is redundant since it is automatically satisfied throughout the interaction. Thus, the adiabatic wall problem is simplified to the solution of the continuity, momentum, and moment of momentum equations. The present solutions for an adiabatic wall are compared with the Lees-Reeves analysis as well as with experimental pressure data for a Mach 6 airflow.

For the highly cooled wall case, the present theory has been compared with experimental measurements of surface pressure and heat transfer for shock-induced separated regions in Mach 10 airflow. The theoretical predictions are in excellent overall agreement with the measurements.

The variation in size, shape, and properties of an interaction region as the strength of the adverse pressure gradient is varied is of considerable importance. A series of calculations was therefore made using the present method to study the change in pressure, heat transfer, and skin friction distributions as the strength of the interaction was varied.

3

The final application of the present theory has been to study conditions under which a flow will just separate, i. e. , the case of incipient separation. Criteria for determining incipient separation in previous experimental studies have been based on changes in the form of the skin friction, pressure, and heat transfer distributions as the strength of the interaction was increased. These criteria, previously based only on experiment, are strongly supported by the present study.

In the next section of this report, the qualitative features of the flow in regions of shock wave - boundary layer interaction are discussed. Theoretical models which have been derived previously to describe these flows are then briefly reviewed. The formulation of the basic equations used in the present analysis and the method by which these equations are solved are described in Section 3. Section 4 contains the application of the analysis to regions of shock wave - boundary layer interaction over an adiabatic wall and with wall heat transfer.

2. BACKGROUND OF THE PROBLEM

2.1 Qualitative Features of the Flow

Before discussing previous analyses, it is appropriate to review briefly certain basic qualitative features of both shock-induced and wedge-induced interactions.

A schlieren photograph and schematic diagram of shock-induced separation, i. e. , separated flow induced by an oblique shock impinging on a laminar boundary layer, is shown in Fig. 1. The externally generated

shock causes a pressure rise which is fed upstream through the subsonic portion of the boundary layer. This causes the boundary layer upstream of the point of shock impingement to thicken under the adverse pressure gradient, finally separating when the skin friction at the surface is reduced to zero. The interaction between the viscous and inviscid flows in the separation region causes a series of compression waves which coalesce to form the separation shock. The externally generated shock is reflected from the separated viscous layer as an expansion fan because the imbedded subsonic separated region cannot sustain a sudden pressure rise. The net pressure rise through the incident shock and expansion fan is small. The incident shock and expansion fan cause the outer inviscid flow adjacent to the separated layer to turn back towards the flat plate. A compression fan is formed as the flow turns parallel to the flat plate which coalesces to form the reattachment shock. The boundary layer reattaches to the plate and continues to thin until the neck region of the interaction is reached, at which point the viscous layer has a local minimum. Downstream of the neck, the viscous layer grows in the adverse pressure gradient until the pressure at the end of the interaction reaches a value equivalent to a compression of the free stream through twice the angle of the shock generator.

Wedge-induced separated regions are similar in many ways to those generated by an external oblique shock. A schlieren photograph and a schematic diagram of the separated flow over a flat-plate wedge model are shown in Fig. 2. The pressure disturbance caused by the wedge is fed upstream through the subsonic portion of the boundary layer causing it to thicken, thus producing a decrease in the momentum of fluid adjacent to

5

the flat plate. The flow separates ahead of the wedge with the formation of a separation shock. Experiment has shown that the shock wave - boundary layer interaction in this region is very similar to the phenomena observed in the externally generated shock-induced flow. Following the strong inter- action in the separation region is a region of approximately constant pres- sure, the plateau pressure, which corresponds to a similar region close to shock impingement in the externally generated shock-induced flow. As the free shear layer approaches the reattachment point it begins to turn parallel to the wedge causing a strong interaction between the viscous and inviscid flows. The compression fan produced in this region coalesces to form the reattachment shock. Downstream of reattachment, the boundary layer reaches a local minimum in the neck region after which it slowly re- verts to a self-similar growth well downstream of the interaction. From isentropic inviscid flow considerations, it is easily shown that the total pressure rise across an interaction induced by a shock generator angle, α , is equal in magnitude to the pressure rise across an interaction on a flat- plate wedge configuration with a wedge angle, 2α . For these geo- metrically equivalent models, experiment has shown that both pressure and heat transfer distributions are very similar. The model proposed here can be used to analyze either of the types of shock-induced separated regions discussed previously.

2.2 Previous Analyses

The previous theoretical studies of separated regions induced by shock wave - boundary layer interaction are based on boundary layer equa- tions. Techniques which had been used to analyze unseparated boundary

layer development were tentatively extended in attempts to analyze separated regions. Because of the complexity of the problem, almost all the approaches have treated the problem using momentum integral methods.

The Karman-Pohlhausen[1] momentum integral method has been used by a number of authors[2,3] to analyze regions of shock-induced separated flow. The basic assumption used in the Karman-Pohlhausen method, namely, that the velocity profiles are uniquely determined by the local pressure gradient parameter $\lambda(x) \left[= \frac{\delta}{\mu U} \frac{dp}{dx} \right]$, results in a Blasius-type profile in the constant pressure separated region between the separation and reattachment points. In contrast, experiment has shown that the flow in the region between separation and reattachment must be characterized by velocity profiles which exhibit reverse flow, and the interaction between the external flow and the viscous separated region must result in the characteristic plateau pressure found in the experimental studies.

As a consequence of the failure of the preceding techniques, subsequent methods have utilized characteristic parameters which are not related directly to the local static pressure distribution. The Crocco-Lees[4] method was the first of such analyses. Rather than directly satisfy the momentum equation at the wall, the authors introduced a conservation equation relating the entrainment of mass from the external inviscid flow into the boundary layer to a mixing rate parameter. Crocco[5], and also Bray, Gadd, and Woodger[3] have used this method to study the properties of shock-induced separated flows, employing the lower branch solutions of the Falkner-Skan equations to specify the mixing rate function. Although the solutions obtained from these analyses were in general agreement with

experimental results, certain anomalies exist, the most obvious a local decrease in the static pressure just upstream of the reattachment compression rise. This dip in the pressure distribution is indicative of an expansion process upstream of shock impingement, a feature not observed in experimental studies.

This discrepancy between theory and experiment was further examined by Glick[6]. He found that if the mixing rate parameter were specified from experiment rather than from the Falkner-Skan solutions, the resulting theoretical pressure distributions were in very good agreement with experiment. Since the mixing rate parameter was determined from a limited amount of experimental data in flows over an adiabatic wall, there is no means of determining "a priori" whether the analysis is valid at different Reynolds number, Mach number, or wall cooling conditions.

To formulate a solution which eliminates the semi-empirical features of Glick's form of the Crocco-Lees technique requires additional basic equations. In this way the momentum equation at the wall, $\left(\frac{dp}{dx} = \frac{d\tau}{dy}\right)$, need not be utilized, and the velocity and enthalpy profiles in the interaction region can be related to independent parameters which are not associated directly with the static pressure distribution. An analysis based on this concept was introduced by Tani[7] who formulated the first moment of momentum (or kinetic energy) equation. Tani used a quartic representation to describe the velocity profiles of an adiabatic flow in an adverse pressure gradient. The nondimensionalized velocity gradient at the wall was chosen as a parameter. Solutions based on Tani's method have been found to be in very good agreement with more accurate methods based on direct

solutions to the partial differential equations of the boundary layer. Poots[8] improved and extended Tani's method to analyze the development of a compressible laminar boundary layer in a prescribed adverse pressure gradient over highly cooled walls. By introducing the energy equation, in addition to the momentum and moment of momentum equations used by Tani, Poots was able to specify an enthalpy profile through the boundary layer. The enthalpy gradient at the wall was chosen to specify a particular quartic profile. Simultaneous solutions to these equations were compared with power series solutions of the corresponding partial differential equations and were found to be in excellent agreement for the case of linearly retarded, highly cooled flow.

Abbott, Holt, and Nielson[9] studied shock-induced separated regions by using the analytical technique developed by Poots. They also used quartic profiles to represent the distribution of velocity in the attached and separated regions of the flow. For adiabatic flows, the theory was in good agreement with experimental measurements of the static pressure up to the separation point. Downstream of separation the theory did not predict the characteristic plateau found in their experiments. In highly cooled flow, the disagreement was more startling since their theory predicted heat transfer from the walls to the flow in the separated region.

Both Savage[2] and Lees and Reeves[10] associated the failure of the method proposed by Abbott, et al, with the assumption of quartic profiles to represent the velocity distribution in an adiabatic separated region. They suggest that the velocity in the separated and attached region would be better represented by a family of solutions based on the compressible

flow analog of the Falkner-Skan equations, or by velocity profiles based on two parameters. The first of these alternatives is used in the latest analysis developed by Lees and Reeves[10]. They utilize the Crocco-Lees form of the continuity equation, the momentum and moment of momentum equations to describe the development of the viscous flow and its interaction with the outer inviscid stream. For attached flows, the velocity and enthalpy profiles are assumed to be a unique function of the nondimensional velocity gradient parameter evaluated at the wall. The profiles are assumed to be independent of the pressure gradient parameter with which they are associated in the Cohen and Reshotko[11] solutions. Lees and Reeves found very good agreement between their theoretical calculations and experimental measurements for shock-induced separated regions over an adiabatic wall in Mach 2.67 and 6 airflows.

Lees and Reeves also reintroduced the concept of supercritical boundary layers originally postulated by Crocco[5]. They found that the laminar boundary layer over a highly cooled wall in hypersonic flow was supercritical in the absence of a pressure gradient. Thus, this boundary layer should thin if an adverse pressure gradient were imposed. Such behavior is in direct contrast to high-speed flow over an adiabatic wall where the boundary layer is subcritical[10] and thus is thickened by an adverse pressure gradient. The result implies that for the flow to separate in a highly cooled laminar boundary layer in hypersonic flow, there must be a sudden transition or jump from the supercritical to the subcritical boundary layer condition ahead of the separated region. Experimental measurements reported by Holden[12] for shock-induced, highly cooled separated regions in

a Mach 10 airflow were for conditions in which the laminar boundary layers in the absence of a pressure gradient were supercritical in the Lees and Reeves formulation. These measurements indicated that the adverse pressure gradient in the separation region was propagated approximately five boundary thicknesses upstream of the separation causing the boundary layer to thicken gradually over this region. Clearly, this represents a discrepancy between theory and experiment.

In the initial stage of the present study this apparent discrepancy was investigated by examining the Lees and Reeves equations governing the definition of subcritical and supercritical flows. Calculations were made with the edge of the boundary layer defined by $f' = 0.95$, 0.99, and 0.995 to determine the integral properties upon which the above equations depend. It was found that these integral properties were inaccurately represented. Further calculations using more accurate integral properties indicated that laminar boundary layers in the absence of a pressure gradient are always subcritical regardless of the magnitude of the wall cooling.

The Lees and Reeves formulation, together with the new integral properties, were then used to calculate the distribution of pressure and heat transfer for comparison with the experimental results in hypersonic highly cooled flows described by Holden[12]. Although the integration proceeded smoothly from the beginning of the interaction through the separation point, the theoretical results were not in agreement with the experimental measurements. The most obvious difference between theory and experiment occurred in the separation region where the experimental measurements showed that the heat transfer decreased below the flat plate

value, whereas the theory predicted an increase in heat transfer in this region.

This discrepancy between theory and experiment can be attributed to the fact that in high Mach number flows over highly cooled walls the energy which is dissipated in and convected across the viscous shear layer significantly influences the development and structure of both the attached and separated shear layer. Thus, it is important that the energy equation be satisfied in this region.

3. PRESENT ANALYSIS

3.1 Formulation of the Integral Equations

Because of the complex nature of the model necessary to adequately describe the flow in the separated and unseparated shear layer, the equations of conservation of mass, momentum, moment of momentum, and energy must be satisfied throughout the interaction. We invoke the usual boundary layer approximation that the pressure gradients normal to the surface are negligible compared to streamwise gradients. Although this assumption is justifiable in the separated region and well upstream and downstream of separation and reattachment, respectively, the flow curvature in the vicinity of the separation and reattachment point of shock-induced separated flows may cause considerable transverse pressure gradients. The validity of the assumption of a relatively small pressure gradient must ultimately be determined by comparison with experiment.

The growth of the shear layer in the region under study is governed by the interaction between the external inviscid flow and the viscous layer. By considering the mass entrained from the inviscid stream into the viscous shear layer, Crocco and Lees[4] obtained the conservation equation

$$\tan \theta = \frac{v_e}{u_e} = \frac{d\delta^*}{dx} - \left[\frac{d}{dx} \ln(\rho_e u_e)\right]\left[\int_0^\delta \frac{\rho u}{\rho_e u_e}\, dy\right] \qquad (3.1)$$

where θ is the local inclination of the streamline at the edge of the boundary layer and v_e and u_e are vertical and horizontal components of velocity, respectively, at a given longitudinal location. Transformation of Eq. (3.1) into the incompressible plane by applying the Stewartson-Illingworth transformation and assuming an isentropic compression process gives

$$\tan \theta = \delta_i^* \, (1 + m_\infty)\left(\frac{m_e}{1+m_e}\right)\left\{\left[H + \left(\frac{m_e+1}{m_e}\right)(1 + S_w t)\right] \frac{d}{dX} \ln \delta_i^* + \right.$$

$$+ \frac{dH}{dX} + \left[2H + \left(\frac{3\gamma-1}{\gamma-1}\right) + \left(\frac{\gamma+1}{\gamma-1}\right)\frac{m_e}{1+m_e} \, H + \left(\frac{3\gamma-1}{\gamma-1}\right)S_w t\right.$$

$$\left. + \frac{M_e^2-1}{m_e(1+m_e)} \, \frac{1}{\delta_i^*}\int_0^{\delta_i} \frac{U}{U_e}\, dY\right]\left[\frac{d}{dX}\ln M_e\right] + \left(\frac{1+m_e}{m_e}\right)\frac{dt}{dX}\, S_w\left.\right\}$$

which, upon simplification, becomes

$$\bar{\tau} \frac{dT}{dX} + \tilde{C}\frac{d}{dX}(\ln \delta_i^*) + \frac{dH}{dX} + F\frac{d}{dX}(\ln M_e) = \frac{-v_\infty}{a_\infty(\delta_i^*)M_e}\, g \qquad (3.2)$$

where

$$\tilde{C} = H + \left(\frac{m_e+1}{m_e}\right)(1 + S_w t)$$

$$F = \left[2H + \left(\frac{3\gamma-1}{\gamma-1}\right) + \left(\frac{3\gamma-1}{\gamma-1}\right) S_w t + \left(\frac{\gamma+1}{\gamma-1}\right) \frac{m_e}{1+m_e} H + \frac{M_e^2-1}{m_e(1+m_e)} \frac{1}{\delta_i^*} \int_o^\delta \frac{U}{U_e} dY \right]$$

$$g = -Re_{\delta_{i_o}^*} \delta_R \left(\frac{M_e}{M_\infty}\right) \frac{(1+m_e)}{m_e(1+m_\infty)} \tan\theta$$

$$W = \frac{1}{\delta_i^*} \int_o^{\delta_i} \frac{U}{U_e} dY \qquad\qquad \bar{\tau} = S_w \left(\frac{1+m_e}{m_e}\right)\left(\frac{dt}{dT}\right) \quad ,$$

and

$$m_e = \frac{(\gamma-1)}{2} M_e^2 ; \qquad H = \frac{\theta_i}{\delta_i^*} ; \qquad T = \frac{K}{\delta_i^*} ; \qquad t = \frac{I}{\delta_i^*} ; \qquad M_e = \frac{U_e}{a_e}$$

where

$$\delta_i^* = \int_o^{\delta_i} \left[1 - \frac{U}{U_e} \right] dY$$

$$\theta_i = \int_o^{\delta_i} \frac{U}{U_e}\left(1 - \frac{U}{U_e}\right) dY$$

$$K = \int_o^{\delta_i} \frac{S}{S_w} \frac{U}{U_e} dY$$

In the present model it is assumed that the interaction between the viscous and inviscid flow causes a series of isentropic compression and expansion waves. Thus, the angle θ of the streamline at the outer edge of the viscous layer is related to the local inviscid flow Mach number, M_e, by the Prandtl-Meyer relationship

$$-\theta = \bar{\nu}(M_e) - \bar{\nu}_{REF}$$

where

$$\bar{\nu}(M_e) = \sqrt{\frac{\gamma+1}{\gamma-1}} \tan^{-1}\left\{ \sqrt{\frac{\gamma-1}{\gamma+1}} \sqrt{M_e^2-1} - \tan^{-1}\sqrt{M_e^2-1} \right\}$$

and $\bar{\nu}_{REF}$ is evaluated at a reference condition where $\theta = 0$.

Therefore,

$$g = Re_{\delta_{i_o}^*} \; \delta_R \left(\frac{M_e}{M_\infty}\right) \frac{(1+m_e)}{m_e(1+m_\infty)} \; \tan\left[\bar{\nu}(M_e) - \bar{\nu}_{REF}\right]$$

Using the usual boundary layer equations

Continuity

$$\frac{\partial}{\partial x}(\rho u) + \frac{\partial}{\partial y}(\rho v) = 0 \tag{3.3}$$

Momentum

$$\rho u \frac{\partial u}{\partial x} + \rho v \frac{\partial u}{\partial y} = -\frac{dp}{dx} + \frac{\partial}{\partial y}\left[\mu \frac{\partial u}{\partial y}\right] \tag{3.4}$$

$$\frac{\partial p}{\partial y} = 0$$

Energy

$$\rho u \frac{\partial h}{\partial x} + \rho v \frac{\partial h}{\partial y} = u \frac{dp}{dx} + \frac{\partial}{\partial y}\left(\frac{\mu}{Pr}\frac{\partial h}{\partial y}\right) + \mu\left(\frac{\partial u}{\partial y}\right)^2 , \tag{3.5}$$

together with Stewartson-Illingworth transformation

$$dX = \lambda \frac{a_e \rho_e}{a_\infty \rho_\infty} dx \qquad \text{and} \qquad dY = \frac{a_e \rho}{a_\infty \rho_\infty} dy$$

$$U = \psi_Y = \frac{\rho u}{\rho_\infty} \quad ; \quad V = -\psi_X = \frac{\rho v}{\rho_\infty} \tag{3.6}$$

where $\mu/\mu_\infty = \lambda(t/t_\infty)$ and (as in Ref. 11) $\lambda = \sqrt{\frac{t_w}{t_\infty}}\left(\frac{t_\infty + k_{sU}}{t_w + k_{sU}}\right)$,

we obtain the analogs of the incompressible form of the boundary layer equations

$$\frac{\partial U}{\partial X} + \frac{\partial V}{\partial Y} = 0 \tag{3.7}$$

$$U \frac{\partial U}{\partial X} + V \frac{\partial U}{\partial Y} = U_e \frac{dU_e}{dX}(1+S) + \nu_\infty \frac{\partial^2 U}{\partial Y^2} \tag{3.8}$$

$$U \frac{\partial S}{\partial X} + V \frac{\partial S}{\partial Y} = \frac{\nu_\infty}{Pr} \frac{\partial^2 S}{\partial Y^2} \qquad (3.9)$$

These equations are reduced to a system of first order, nonlinear, ordinary differential equations by integrating each equation, term by term, across the thickness of the boundary layer. Thus, we generate the integral forms of the boundary layer equations.

Integrating Eq. (3.8) across the boundary layer and using Eq. (3.7), we obtain

$$U_e \frac{d(\theta_i)^2}{dX} + 2 \left[2 + \frac{\delta_i^*}{\theta_i} + \frac{S_w I}{\theta_i} \right] \theta_i^2 \frac{dU_e}{dx} = \frac{2 \nu_\infty \theta_i}{U_e} \left[\frac{\partial U}{\partial Y} \right]_{Y=0} , \qquad (3.10)$$

the integral form of the momentum equation.

Integrating Eq. (3.9) across the boundary layer and using Eq. (3.7), we obtain the integral form of the energy equation

$$U_e \frac{d(K)^2}{dX} + 2K^2 \frac{dU_e}{dX} = -2 \nu_\infty K \frac{d}{dY} \left(\frac{S}{S_w} \right)_{Y=0} \qquad (3.11)$$

Multiplying the momentum Eq. (3.8) by U and integrating across the boundary layer, we obtain the kinetic energy or moment of momentum equation

$$U_e \frac{d(\theta_i^*)^2}{dX} + 2 \left(3 + \frac{2 S_w K}{\theta_i^*} \right) \theta_i^{*2} \frac{dU_e}{dX} = 4 \frac{\nu_\infty \theta_i^*}{U_e^2} \int_0^\delta \left(\frac{dU}{dY} \right)^2 dY \qquad (3.12)$$

where

$$\theta_i^* = \int_0^{\delta_i} \frac{U}{U_e} \left[1 - \left(\frac{U}{U_e} \right)^2 \right] dY$$

Rewriting these equations into a form similar to the continuity, Eq. (3.2), gives

$$H \frac{d}{dX} \ln \delta_i^* + \left[2H + 1 + S_w t \right] \frac{d}{dX} \ln M_e + \frac{dH}{dX} = \frac{\nu_\infty}{a_\infty M_e (\delta_i^*)^2} P \qquad (3.13)$$

16

$$J \frac{d}{dX} \ln \delta_i^* + \left[3J + 2S_w T \right] \frac{d}{dX} \ln M_e + \frac{dJ}{dH} \frac{dH}{dX} = \frac{\nu_\infty}{a_\infty M_e (\delta_i^*)^2} R \quad (3.14)$$

$$T \frac{d}{dX} \ln \delta_i^* + T \frac{d}{dX} \ln M_e + \frac{dT}{dX} = - \frac{\nu_\infty}{a_\infty M_e (\delta_i^*)^2} Q \quad , \quad (3.15)$$

the momentum, kinetic energy, and energy equations, respectively, where

$$J = \frac{\theta_i^*}{\delta_i^*} ; \qquad P = \frac{\delta_i^*}{U_e} \left(\frac{dU}{dY} \right)_{Y=0} ; \qquad R = \frac{2\delta_i^*}{U_e^2} \int_0^{\delta_i} \left(\frac{\partial U}{\partial Y} \right)^2 dY$$

$$Q = \frac{d}{dY} \left(\frac{S}{S_w} \right)_{Y=0} \delta_i^* ; \qquad T = \frac{K}{\delta_i^*} \qquad \text{and} \qquad t = \frac{I}{\delta_i^*}$$

Equations (3.2), (3.13), (3.14), (3.15) are four simultaneous, nonlinear, ordinary differential equations which are functions of the displacement thickness, δ_i^*, the Mach number, M_e, just outside the boundary layer, and the velocity and enthalpy profiles.

Solving these equations simultaneously, we obtain

$$\frac{\delta_i^*}{M_e} \frac{dM_e}{dX} = \frac{1}{\left(\frac{a_\infty M_e \delta_i^*}{\nu_\infty} \right)} \frac{M_1(H, T, M_e, q)}{C(H, T, M_e)} \quad (3.16)$$

$$\delta_i^* \frac{dH}{dX} = \frac{1}{\left(\frac{a_\infty M_e \delta_i^*}{\nu_\infty} \right)} \frac{M_2(H, T, M_e, q)}{C(H, T, M_e)} \quad (3.17)$$

$$\frac{d\delta_i^*}{dX} = \frac{1}{\left(\frac{a_\infty M_e \delta_i^*}{\nu_\infty} \right)} \frac{M_3(H, T, M_e, q)}{C(H, T, M_e)} \quad (3.18)$$

17

$$\delta_{\dot{\iota}}^{*} \frac{dT}{dX} = \frac{1}{\left(\dfrac{a_{\infty} M_e \delta_{\dot{\iota}}^{*}}{\nu_{\infty}}\right)} \frac{M_4(H,T,M_e,g)}{C(H,T,M_e)}$$

<div style="text-align:right">(3.19)</div>

where

$$M_1 = \bar{\tau}\left\{ T\left(P\frac{dJ}{dH} - R\right) + Q\left(H\frac{dJ}{dH} - J\right)\right\} + \left(\frac{m_e+1}{m_e}\right)(1+S_w t)\left(R - P\frac{dJ}{dH}\right)$$
$$+ (P+g)\left(J - H\frac{dJ}{dH}\right)$$

$$M_2 = \bar{\tau}\left\{ T\left[R(H+1+S_w t) - P(2J+2S_w T)\right] + Q\left[J(H+1+S_w t)\right.\right.$$
$$\left.\left. - H(2J+2S_w T)\right]\right\} + \left[\frac{m_e+1}{m_e}\right](S_w t+1)\left[(3J+2S_w T)P\right.$$
$$\left. - R(2H+1+S_w t)\right] + (P+g)\left[H(3J+2S_w T) - FJ\right]$$
$$+ \left[F - (2H+1+S_w t)\right]\left[RH + J_g\right]$$

$$M_3 = \bar{\tau}\left\{ Q\left[-(2H+1+S_w t)\frac{dJ}{dH} + (3J+2S_w T)\right] + T\left(R - P\frac{dJ}{dH}\right)\right\}$$
$$+ (P+g)\left[F\frac{dJ}{dH} - (3J+2S_w T)\right]$$
$$- \left[F - (2H+1+S_w t)\right]\left[R + g\frac{dJ}{dH}\right]$$

$$M_4 = \left(\frac{m_e+1}{m_e}\right)(1+S_w t)\left\{\frac{dJ}{dH}\left[(2H+1+S_w t)Q + PT\right]\right.$$
$$\left. - \left[TR + Q(3J+2S_w T)\right]\right\} + \left[F - (2H+1+S_w t)\right]\left[JQ + TR\right.$$
$$\left. - \frac{dJ}{dH}(HQ+PT)\right] + (P+g)T\left[(2J+2S_w T) - \frac{dJ}{dH}(H+1+S_w t)\right]$$

$$C = \bar{r} T \left[(H + 1 + S_w t) \frac{dJ}{dH} - (2J + 2S_w T) \right]$$

$$+ \left(\frac{m_e + 1}{m_e} \right)(1 + S_w t) \left[(3J + 2S_w T) - (2H + S_w t + 1)\frac{dJ}{dH} \right]$$

$$+ \left[(2H + 1 + S_w t) - F \right] \left[J - H \frac{dJ}{dH} \right]$$

The integral parameters, H, J, T, t, etc., are functions of the velocity and enthalpy profiles. Therefore, before we can evaluate these parameters, we must first select a system of velocity and enthalpy profiles to represent the form and development of the flows in attached and separated shock-induced regions. Further, these profiles must be related to parameters of intrinsic importance to the problem.

3.2   The Velocity and Enthalpy Profiles

The integral equations can be solved only if the velocity and enthalpy profiles can be prescribed. In the conventional application of the momentum integral technique, the distribution of velocity and temperature are represented by polynomials. The quartic representation introduced by Tani[7] is one form which has been used successfully in a number of analyses [7,8] to describe the development of an attached layer in an adverse pressure gradient. As described in Sec. 2.2, Abbott, Holt, and Nielson[9] attempted to use this representation to describe the boundary layer development in an adverse pressure gradient induced by shock wave - boundary layer interaction in an adiabatic flow. Although their solutions were in good agreement with experimental

measurements up to the separation point, the calculations predicted a peak pressure in the separated region just upstream of the reattachment compression process which was inconsistent with the results of experimental studies, including their own. Lees and Reeves showed later that this anomalous pressure distribution in the separated region was an inherent feature of the single parameter quartic representation. Measurements by Hakkinen et al[13] of the distribution of velocity in a shock-induced separated region showed that when the boundary layer separates from the surface, the shape of the velocity profile above the zero velocity streamline is preserved as the shear layer grows. However, the velocity profile in the reverse flow region develops in a nonsimilar manner, with the maximum velocity in this region first increasing and then decreasing as the velocity distribution changes in form. A velocity distribution based on a single parameter polynomial profile cannot be expected to represent the complex development of this viscous layer. A more accurate representation of the distribution of velocity in the separated region could be achieved by introducing polynomial profiles dependent on two or more parameters, or by representing the velocity above and below the zero velocity streamline by a different family of profiles. In either case, we require a further moment of momentum equation to specify the second parameter, thereby introducing further complexity into an already complex situation.

Lees and Reeves[10] found that the lower branch solutions to the Falkner-Skan equations gave velocity profiles with reverse flow which exhibited approximately the same form as those found in experiment. By relating the velocity profiles to the nondimensionalized velocity gradient at the surface rather than to the pressure gradient with which they are associated in the Falkner-Skan solutions, they found that the qualitative development of the profiles in the separated region was in agreement with experiment. By linking the velocity and the enthalpy profiles through the solution to the Falkner-Skan equations, they were able to obtain a single-parameter family of profiles to represent the flow in attached and separated regions.

The Falkner-Skan solutions which represent the incompressible boundary layer development over a wedge were generalized by Cohen and Reshotko[11] to describe these boundary layers in compressible flow. By defining the variation of velocity in the external flow field by $U_e = c x^{m}$ and choosing similarity parameters

$$\psi = f(\eta) \sqrt{\frac{2}{m_e + 1} \, \nu_\infty \, U_e \, x}$$

$$\eta = \frac{Y}{X} \sqrt{\frac{m_e + 1}{2} \, \frac{U_e \, X}{\nu_\infty}} \qquad ,$$

the boundary layer equations reduce the ordinary differential equations

$$\frac{d^3 f}{d\eta^3} + f \frac{d^2 f}{d\eta^2} + \beta \left[1 - S - \left(\frac{df}{d\eta}\right)^2 \right] = 0 \qquad (3.20)$$

21

$$\frac{d^2 S}{d\eta^2} + f \frac{dS}{d\eta} = 0$$

(3.21)

where $\Pr = 1$, $\beta = \left[2m/m + 1\right]$ and $f' = \frac{U}{U_e} = \frac{u}{u_e}$.

A series of numerical solutions to these equations were obtained by Cohen and Reshotko[11] for a number of wall-to-free stream temperature ratios and a series of values of the pressure gradient parameter β . Two physically meaningful classes of solutions are found to exist for the flow profiles in an adverse pressure gradient with $(dU/dY)_w \geq 0$. The lower branch solutions are typical of separated flow profiles with a region of reverse flow adjacent to the wall, and thus are characterized by $(dU/dY)_w < 0$.

Here, we use the Cohen and Reshotko solutions to the Falkner-Skan equations to describe the distribution of velocity and enthalpy in the attached and separated viscous regions of the shock wave-boundary layer interaction. We decouple the velocity profiles from the pressure gradient parameters with which they are associated in Cohen and Reshotko's solutions and relate them to the parameter a (X) which is defined as $\frac{1}{\delta_i^*} \left| \frac{\partial U/U_e}{\partial Y/\delta_i} \right|_w$ for attached flow and Y^*/δ_i^* for separated flow, where Y^* is the distance between the wall and the point of zero velocity in the shear layer. We further decouple the enthalpy profiles from the pressure gradient parameters and the velocity profiles and relate them to the parameter b(X) which is defined as $\frac{-\partial}{\partial Y} \left[\frac{S}{S_w}\right]_w$, the enthalpy gradient at the wall in both attached and separated flows. By specifying both a (X) and b(X), we define a unique

pair of velocity and enthalpy profiles and also the integral properties associated with these profiles.

3.3   The Integral Parameters

Now that the forms of the velocity and enthalpy profiles have been selected and can be prescribed in terms of two independent variables, a and b, the integral parameters, H, J, K ....can be evaluated. These parameters, which were calculated from the Cohen and Reshotko solution[11], were fitted in terms of a power law series in a and b by the method of least mean squares. The functions G, H, J, Z, P, R, which are velocity dependent, were fitted as a power series in a and are of the form

$$H = c_o + c_1 a^2 + c_2 a^2 + \cdots \cdot c_n a^n$$

These coefficients are listed in Table I.

The functions T, t, and Q are functions of both a and b. We write

$$T = \frac{\int_o^{\delta_i} \frac{s}{S_w}\left(\frac{U}{U_\infty}\right) dY}{\int_o^{\delta_i}\left(1 - \frac{U}{U_\infty}\right) dY} = \frac{K(a, b)}{G(a)}$$

$$t = \frac{\int_o^{\delta_i} \frac{s}{S_w} dY}{\int_o^{\delta_i}\left(1 - \frac{U}{U_\infty}\right) dY} = \frac{I(b)}{G(a)}$$

$$Q = \frac{d}{dY}\left(\frac{s}{S_w}\right) \int_o^{\delta_i}\left(1 - \frac{U}{U_\infty}\right) dY = -b\, G(a)$$

The function I which is expressed as polynomials in b is also shown in Table I. We have expressed K, a function of both a and b, in the form

23

$$K_{a=r} = c_{0,r} + c_{1r} b + c_{2r} b^2 + c_{3r} b^3$$

where r goes from zero to 1.60 in intervals of 0.1. The value of K is obtained by single interpolation between the curves of constant a. The partial derivative of K with respect to b is written in the form

$$\frac{\partial K}{\partial b}\bigg|_{a=r} = c_{1r} + 2c_{2r} b + 3c_{3r} b^2$$

The value of this again is obtained by double interpolation between curves of constant a. To determine the partial derivatives of K with respect to a, Table II is used and $\frac{\partial K}{\partial a}$ is determined using a similar double interpolation technique from the form

$$\frac{\partial K}{\partial a}\bigg|_{b=r} = d_{1r} + 2d_{2r} a + 3d_{3r} a^2$$

Rewriting Eqs. (3.2), (3.13), (3.14), and (3.15), we have

$$\frac{\delta_R}{M_e} \frac{dM_e}{dX} = \frac{1}{\tilde{R}e_{\delta_{i_0}}} \left\{ M_1(H,T,M_e,g) \bigg/ C(H,T,M_e) \right\} \tag{3.21}$$

$$\delta_R\left(\frac{da}{dX}\right) = \frac{1}{\tilde{R}e_{\delta_{i_0}}} \left\{ M_2(H,T,M_e,g) \bigg/ C(H,T,M_e) \right\}\left(\frac{dH}{da}\right)^{-1} \tag{3.22}$$

$$\delta_R\left(\frac{db}{dX}\right) = \frac{1}{\tilde{R}e_{\delta_{i_0}}} \left\{ M_4(H,T,M_e,g) \bigg/ C(H,T,M_e) \right\}\left(\frac{dT}{db}\right)^{-1} \tag{3.23}$$

$$\frac{d\delta_i^*}{dX} = \frac{1}{\tilde{R}e_{\delta_{i_0}}} \left\{ M_3(H,T,M_e,g) \bigg/ C(H,T,M_e) \right\} \tag{3.24}$$

where

$$\delta_R = \frac{\delta_i^*}{\delta_{i_0}^*} \quad ; \qquad \alpha^2 = \left[\frac{\delta_{i_0}^*}{X_0} \sqrt{\frac{m+1}{2} \frac{UX_0}{\nu_\infty}}\right]^2$$

24

and

$$\frac{db}{da} = \frac{M_4 G \frac{dH}{da} + \frac{C_1 I}{G}\left(\frac{dG}{da}\right) - C_2\left[\frac{\partial K}{\partial a} - \frac{K}{G}\frac{dG}{da}\right]}{C_1 \frac{dI}{db} + C_2 \frac{\partial K}{\partial b}}$$

$$C_1 = S_w \left(\frac{m_e + 1}{m_e}\right)\left\{ T\left[R(H+1+S_w t) - P(2J + 2S_w T)\right] + Q\left[J(H+1+S_w t) - H(2J+2S_w T)\right]\right\}$$

$$C_2 = \left(\frac{m_e + 1}{m_e}\right)(1+S_w t)\left[(3J+2S_w T)P - R(2H+1+S_w t)\right] + (P+Q)\left[H(3J+2S_w T) - FJ\right]$$

$$+ \left[F - (2H+1+S_w t)\right]\left[RH + JF\right]$$

Also

$$\frac{dT}{db} = \left[\frac{\partial K}{\partial a}\frac{1}{G} - \frac{K}{G^2}\frac{dG}{da}\right]\frac{1}{\left(\frac{db}{da}\right)} + \frac{1}{G}\frac{\partial K}{\partial b}$$

$$\frac{dt}{dT} = \frac{-I\frac{dG}{da} + G\frac{dI}{db}\left(\frac{db}{da}\right)}{\left[\left(G\frac{dK}{da} - K\frac{dG}{da}\right) + G\frac{\partial K}{\partial b}\frac{db}{da}\right]}$$

Equations (3.21), (3.22), (3.23), (3.24) are the differential equations which are solved simultaneously to yield the variation of the basic parameters a, b, M_e, and δ_R.

3.4   Technique for Solving the Integral Equations

To obtain detailed distributions of the properties throughout the separated region, it is necessary to integrate the four nonlinear, simultaneous, ordinary differential Eqs. (3.21), (3.22), (3.23) and (3.24). A solution to these equations can be found by prescribing the free stream Mach number upstream and downstream of the interaction and free stream Reynolds

number based on the distance from the leading edge to the beginning of the interaction. We integrate these equations using the Adams-Moulton predictor-corrector method with the Runge-Kutta method for starting the calculation.

The integration of the equations is divided into a number of distinct phases. These cover the regions (a) from the beginning of the interaction to the separation, (b) from separation to the point of maximum displacement thickness, (c) from a maximum displacement thickness to reattachment, and (d) from reattachment to downstream of the interaction passing through the neck region.

(a)   Integration from the beginning of the interaction to the separation point

In the high Mach number-low density regime, there is an interaction between the growth of the boundary layer and the outer inviscid flow--the boundary layer displacement effect--upstream of the main interaction under study. This secondary interaction causes the local inviscid flow Mach number ahead of the interaction to be slightly less than the Mach number of the free stream. The profiles of velocity and enthalpy will also differ slightly from the constant pressure Blasius profiles. Because we assume that the boundary layer profiles upstream of the main interaction are self similar, the derivatives of M_e, a and b with respect to δ^* must tend to zero at the beginning of the interaction, thus M_1 and M_2 (see pp. 17 and 18) go to zero as $a \longrightarrow a$ (Blasius). Expressing M_1 and M_2 in terms of δ_t^*, as given by Lees and Reeves, it is easily shown that if M_1 and M_2 go to zero, then $R_t H_t = P_t J_t$ and hence,

$$(\mathcal{g})_0 = -\left(\frac{1+m_o}{m_o} + H_t\right) \frac{P_t}{H_t}$$

and

$$(\mathcal{g})_0 = -Re_{\delta_t^*} \frac{M_e}{M_\infty} \left(\frac{1+m_o}{m_o}\right) \frac{tan\left(\nu_\infty - \nu\,[M_o]\right)}{\left(1+m_\infty\right)}$$

The values of a and b at the beginning of the interaction were determined by iteration such that $M_1 = M_2 = M_3 = M_4 = 0$ and $C \neq 0$.

The integration scheme was initiated with the values of a, b, and M_o obtained in the manner explained above at the point $\delta_R = \left(\frac{\delta_i^*}{\delta_{i_o}^*}\right) = 1$. Equations (3.21), (3.22), (3.23), and (3.24) were integrated downstream with X as the independent variable, using the integral parameters determined from the unseparated profiles, until the separation point was reached at which point $a = 0$.

(b)   Integration from separation to the point of maximum displacement thickness

The integration scheme is re-initiated at $a = 0$ with the values obtained for δ_{sep}, b_{sep} and M_{sep}, together with the integral parameters determined from the separated velocity and enthalpy profiles. Integration proceeds with increasing δ_R until a reaches an initially prescribed value a_{stop}. This value of a is related directly to the size of the separated region and the total pressure rise across the interaction. This initial value for a_{stop} is a trial value. By successive iterations on this parameter, we are able to match the condition prescribed from inviscid flow relations downstream of the interaction.

(c)   Integration from maximum displacement thickness to the
        reattachment point

The Mach number is continuous across the point of maximum boundary layer displacement thickness. The integration is re-initiated at this point, using the final values for a, b, δ_R, and M_e obtained in the preceding phase. The expression for g is rewritten in terms of the downstream conditions

$$ g = Re_{\delta_{i_0}^*} \; \delta_R \; \frac{M_e}{M_{e2}} \left(\frac{1 + m_e}{m_e} \right) \frac{tan \left(\bar{\nu} [M_e] - \bar{\nu}_{e2} \right)}{1 + m_{\infty}} \; . $$

The integration is continued with decreasing δ_R until the reattachment point is reached where a is again zero.

(d)   Integration from the reattachment point to downstream of the inter-
        action

Downstream of reattachment, the integration scheme uses the attached profile characteristics. As the integration proceeds, δ_R and M_e decrease, a and b increase towards a local minimum in the boundary layer thickness--the neck region of the flow. At this point M_3 is zero. Downstream of the neck, a, b, and δ_R increase and the Mach number decreases with increasing X. The integration is terminated when M_1, M_2 and $M_4 \longrightarrow 0$ as $a \longrightarrow a$ (Blasius); at this point the value of the Mach number is compared with the reference value of the Mach number determined from inviscid flow considerations over the configuration studied; the solution is iterated by changing a_{stop} until an identity is obtained.

4. APPLICATIONS OF THE ANALYSIS

Here, we consider the application of the analysis to study shock-induced flow over an adiabatic wall and the general problem of shock wave - boundary layer interaction with wall heat transfer.

4.1 Shock Wave-Boundary Layer Interaction Over an Adiabatic Wall

For the limiting case of shock-induced separated flow over an adiabatic wall, the equations governing the development of the interaction region reduce to their simplest form. In an adiabatic flow, the energy equation is satisfied identically throughout the flow. Thus, S, S_w, and b are zero in the interaction region. The method reduces to the solution of the continuity, momentum, and moment of momentum integral equations. Putting $S_w = 0$ in the expressions for the derivatives of M_e, δ_R, b, and a with respect to X, we obtain

$$\frac{dM_e}{dX} = \frac{N_1}{D} \tag{4.1}$$

$$\frac{da}{dX} = \frac{N_2}{D} \left[\frac{dH}{da}\right]^{-1} \tag{4.2}$$

$$\frac{d\delta_i^*}{dX} = \frac{N_3}{D} \tag{4.3}$$

where

$$M_1 = N_1 = \left(\frac{m_e+1}{m_e}\right)\left(R - P\frac{dJ}{dH}\right) + (P+g)\left(J - H\frac{dJ}{dH}\right)$$

$$M_2 = N_2 = \left(\frac{m_e+1}{m_e}\right)\left[3PJ+(2H+1)R\right] + (P+g)(3JH-FJ)$$
$$+ \left[F-(2H+1)\right]\left[RH+Jg\right]$$

$$M_3 = N_3 = (P+g)\left(F\frac{dJ}{dH}-3J\right) - \left[F-(2H+1)\right]\left[R-g\frac{dJ}{dH}\right]$$

$$C = D = \left(\frac{m_e+1}{m_e}\right)\left[3J-(2H+1)\frac{dJ}{dH}\right] - \left[F-(2H+1)\right]\left[J-H\frac{dJ}{dH}\right]$$

These relationships are similar to those proposed by Lees and Reeves for analyzing shock-induced separated flow over an adiabatic wall. Because we intend to analyze both attached and separated interaction regions, we specify the Reynolds number at the beginning of the interaction rather than use the Mach number at separation as an input quantity. Thus, the integration scheme described in Sec. 3.4 differs from that proposed by Lees and Reeves.

As a check on the integration technique, a comparison was made with the calculations of Lees and Reeves for shock-induced separated flow on an adiabatic wall. Figure 3 shows a comparison of the variation of δ_R, a, and M_e with Reynolds number based on distance from the leading edge obtained from the two solutions. The results are in very good agreement. The slight difference between the solutions probably results from a slight difference in the R_{x_0} used. Pressure, $\delta_i^* / \delta_{i_0}^*$ and skin friction distributions obtained from these solutions and presented in Figure 4 indicate that the quantities derived from the basic variables are somewhat less sensitive to the accuracy of the calculation than the basic variables

themselves.

Calculations based on the solutions of Eqs. (4.1), (4.2), and (4.3) have been shown[10] to be in good agreement with experimental pressure measurements[13, 14] over an adiabatic wall.

4.2   Shock Wave Boundary Layer Interaction with Wall Heat Transfer

4.2.1   General Nature of the Present Solution and Comparison with Experiment

The present general solution of the shock wave-boundary layer interaction for a highly cooled wall satisfies simultaneously the integral forms of the continuity, momentum, moment of momentum, and energy equations throughout the interaction. From such a solution, the displacement thickness δ_i^*, the local inviscid flow Mach number M_e, and a and b, the parameters which characterize the velocity and enthalpy profiles, are obtained.

A typical variation of these parameters in the interaction region in highly cooled hypersonic airflow is shown in Figure 5. As the attached boundary thickens under the presence of the negative Mach number gradient, the skin friction at the wall, of which a is a measure, decreases and the enthalpy gradient b, a measure of the heat transfer, also decreases. In this formulation of the boundary layer equations, laminar boundary layers, in the absence of a pressure gradient, are subcritical regardless of the degree of wall cooling. The boundary layer separates when $a = 0$; a is redefined in the separated region ($a = Y^*/\delta_i^*$) and, in consequence, describes the path of the zero velocity streamline in this region. As the

boundary layer separates, M_e and b continue to decrease until at the point

of shock impingement b reaches a minimum, and the Mach number gradient

is small (reflecting a region of approximately constant pressure--the

plateau pressure). At reattachment, a is again zero and b returns to

approximately the value which it held at the separation point. The Mach

number gradient, which reaches a maximum at the reattachment point,

reflects the strong interaction in the reattachment region. At the end of

the interaction, the profile parameters a and b approach those corres-

ponding to the constant pressure attached profile (the Blasius profiles) and

the Mach number asymptotes to the value derived from inviscid flow

calculations.

Once a solution has been obtained in terms of the basic parameters

M_e, a , b, and δ_i^*, it is a simple matter to deduce the variation of

pressure

$$\frac{p}{p_o} = \left[\frac{1 + m_o}{1 + m_e} \right]^{(\gamma/\gamma-1)} \tag{4.4}$$

heat transfer

$$\frac{q}{q_o} = \left[\frac{1 + m_o}{1 + m_e} \right]^{\frac{3\gamma-1}{2(\gamma-1)}} \frac{1}{\delta_R} \frac{G}{G_o} \frac{b}{b_o} \tag{4.5}$$

and skin friction

$$\frac{c_f}{c_{f_o}} = \frac{p}{p_o} \frac{P_{(a)}}{P_{(a_o)}} \frac{1}{\delta_R} \tag{4.6}$$

The distribution of heat transfer and pressure calculated from the

parameters, M_e, δ_R , a ,and b, is shown in Figure 6. Here, both

Prandtl-Meyer and linearized theory have been used to relate the distribution

32

of inviscid flow Mach number to the local inclination of the outer edge of the viscous shear layer. For the example shown here, there is little difference between calculations based on the two representations. Also shown for comparison in Figure 6 are the heat transfer measurements by Holden[12] and pressure measurements by Needham[15] on Mach 10 airflows.

The calculated pressure distribution is in very good agreement with the experimental values. It is interesting to note that for this calculation the pressure rise to separation is approximately one-half of the pressure rise to shock impingement, and the separation point occurs at the inflexion point of the pressure distribution in that region. These features have been observed experimentally in laminar shock-induced separated flows over a range of free stream conditions and, in some studies, have been used to define the separation point.

The calculated heat transfer distribution is in good agreement with experimental values in the attached flow region, but the theory underestimates the decrease in heat transfer in the separated region. The theoretical analysis presented here indicates that the point of minimum heat transfer is coincident with the point of maximum displacement thickness. Although the measurements given here and those reported by Bogdonoff and Vas[16] substantiate this feature, similar measurements in shock-induced flow by Miller, Hyman, and Childs[17] indicate that the point of minimum heat transfer occurs at the separation point. The latter work indicates that separation occurs almost at the end of the rise to the plateau pressure.

The reattachment theory proposed by Chapman[18] assumes that reattachment occurs at the end of the pressure rise in the reattachment region.

The calculations presented here indicate that the reattachment pressure ratio $\dfrac{P_r - P_{plateau}}{P_{final} - P_{plateau}}$ is more nearly one-half as compared to Chapman's value of unity. Lees and Reeves showed that Chapman's assumption was equivalent to ignoring the shear gradient, $d\tau/dy$, across the dividing streamline. The position of the point of maximum heat transfer in the reattachment region was found in all calculations to be coincident with the end of the reattachment pressure rise. The experimental evidence presented here and in Refs. 12 and 17 also substantiate this result. The heat transfer rate at the reattachment point is only a fraction of the maximum value.

Two further comparisons between the theory and measurements for wedge separated flows are shown in Figures 7 and 8. In these calculations, the effect of the interaction between the compression fan generated in the separation region and the reattachment compression process is not considered. Figure 7 shows the theoretical and experimental distributions of pressure and heat transfer in the unseparated flow over a flat-plate wedge model. To obtain this solution, the computer program was modified to incorporate an iteration logic described in Sections 3 and 4 capable of working with both attached and separated profiles at the point of maximum displacement thickness. The theoretical pressure and heat transfer distributions are in close agreement with both the form and magnitude of the experimental values. The cusp-like shape of the experimental heat transfer distribution in the region of maximum displacement thickness is displayed in the calculations. However, as noted earlier, the theory tends to underestimate the decrease in heat transfer rate in this region. The calculated pressure distribution also has

the uniform rise through the interaction characteristically found in shock-induced attached flows.

A comparison between the theory and measurements in a well separated flow is shown in Figure 8. The calculated pressure and heat transfer distributions are again in close agreement with the experimental values despite the fact that the form of the distributions now differs markedly from the attached-flow profiles. The pressure distribution now exhibits a region of approximately constant pressure bounded by the large pressure gradients in the separation and reattachment regions while the distribution of heat transfer has the concave form in the plateau region typically found in well separated flows.

4.2.2 The Development of Regions of Shock-Induced Separated Flows

A series of calculations was made to study the variation of shape and size of the pressure, heat transfer, and skin friction distribution as the strength of the adverse pressure gradient causing the interaction was varied. The results of this study are shown in Figure 9 for shock generator angles between 3.95 and 6.25 degrees. The interaction caused by the 3.95° generator angle was of insufficient strength to cause the flow to separate, as can be seen from the skin friction distribution shown in Figure 9a. When the angle of the shock generator is increased, the flow separates, with the resulting region of reverse flow indicated by the negative skin friction coefficients on the surface of the flat plate. These calculations and those for adiabatic flows (Figure 4) indicate that in large separated regions the skin friction coefficient in the reverse flow region is approximately

constant at a small fraction of the attached flow value at the beginning of the interaction. The form and development of the skin friction distributions are in qualitative agreement with skin friction measurements made in shock-induced attached and separated flows by Hakkinen, Greber, Trilling, and Abarbanel[13].

As the strength of the incident shock is increased, the pressure disturbance propagates forward from the point of shock impingement. The character of the pressure distribution changes from an approximately linear rise through the attached interaction region to a form characteristic of separated flows. This form is typified by strong pressure gradients in the separation and reattachment regions bounding the region of approximately constant pressure (the plateau pressure) at the foot of shock impingement.

The theoretical development of the distribution of heat transfer in externally generated shock-induced flow is shown in Figure 9c. Shown for comparison in Figure 10 are experimental heat transfer distributions in wedge- and shock-induced interactions given in Ref. 12. It is apparent from a comparison between the two figures that the qualitative development of the interaction region described by the theoretical model closely parallels the development observed in the experiments. The most striking feature of the analysis is that it predicts the change in character of the heat transfer profiles from a cusp-like distribution in the attached flow to a rounded concave form when the flow is well separated. These changes in the form of the pressure and heat transfer as the boundary layer goes from the attached to the separated condition have been used in experimental programs[12] as criteria to detect incipient separation.

4.2.3 Incipient Separation

Incipient separation occurs when the strength of the interaction is just sufficient to cause the boundary layer to separate. Under this condition there is one point only in the interaction region at which the skin friction is zero. In a well-separated region, the skin friction is zero at both the separation and reattachment points; at the incipient condition these points are coincident. Because it is difficult to make accurate skin friction measurements in high-speed tunnels, other separation criteria have been proposed which are based on more easily measured quantities, such as pressure and heat transfer.

An examination of measured pressure distribution in regions of shock-induced separated flows has indicated that a well-separated flow is characterized by a region of approximately constant pressure (the plateau pressure) in the region of shock impingement. As the severity of the adverse pressure gradient promoting separation decreases, so the size of the plateau region becomes smaller until, in an attached interaction region, the pressure rises in a uniform manner throughout the interaction. The incipient separation condition has been defined experimentally by locating the condition under which the plateau region is vanishingly small, i.e., reduced to an inflexion in the pressure distribution. Another separation criterion tentatively suggested on the grounds of experimental evidence was based on observing a change in the form of the distribution of heat transfer in the interaction region as the strength of the interaction was varied. Measurements have indicated that the incipient separation condition coincides with a change in heat transfer distribution from a cusp-like profile, typical

37

of the profiles in attached flows, to the rounded concave form observed in well-separated regions. Both of these criteria have been developed from experimental observation without any firm backing based on theoretical analysis.

The pressure and heat transfer distribution calculated from the present theory, and shown in Figure 9, exhibit the characteristic trends which have been observed in the experimental studies. The plateau pressure region which typifies a well-separated flow, shrinks as the strength of the interaction decreases, to a mere inflexion in the pressure distribution for conditions close to incipient separation. The rounded form of the heat transfer profiles in the region of shock impingement is a well-separated flow change to a cusp-like form at incipient separation. Thus, this theoretical evidence substantiates, for the first time, the separation criteria based on observation from experiment.

A computer program was formulated to calculate the strength of the free interaction required to cause the incipient separation of a laminar boundary layer in a flow at a given Mach number and Reynolds number. This program was used to calculate the angle of the shock generator required to cause incipient separation at the free-stream conditions (Re = 1.35 x 10^5/in; M_∞ = 10, S_w = -0.8) in the experimental studies reported in Ref. 12. A generator angle of 3.95° was calculated to produce incipient separation; the distributions of pressure, skin friction and heat transfer for this condition are shown in Figure 9. The shock generator angle determined from experiments with wedge- and shock-induced interactions for these conditions was 4.2°. This good agreement between theory and experiment

tends to justify the use of the integral representation and the Cohen and Reshotko velocity and enthalpy profiles to describe the development of an attached boundary in an adverse pressure gradient. Further, this agreement implies that for the flows studied, the pressure gradient developed normal to the surface is not the dominant factor in the mechanism of boundary layer separation in a free interaction.

5. CONCLUSIONS

An analysis has been formulated which describes the laminar viscous and inviscid flow fields in regions of highly cooled shock wave-boundary layer interaction. In this method the integral forms of the continuity, momentum, moment of momentum, and energy equations are used to describe the development of the viscous layer and its interaction with the outer inviscid stream. These equations are solved simultaneously by numerical integration to yield a continuous solution over the entire interaction. The analysis has been compared with experimental measurements in regions of shock wave-boundary layer interaction in hypersonic air flows over adiabatic walls and with heat transfer.

For the limiting case of shock-induced separated flows over an adiabatic wall, the energy equation is redundant since it is satisfied automatically throughout the interaction. The problem is thus simplified to a solution of the continuity, momentum, and moment of momentum equations. The present solutions for the Mach 6 adiabatic flow are in excellent agree-

ment with the Lees and Reeves analysis and also with the experimental pressure data.

The theoretical analysis has been compared with experimental studies of highly cooled regions of shock wave-boundary layer interaction induced by shock impingement on a laminar boundary layer, and by the adverse pressure gradient developed at a flat-plate wedge junction. Theoretical heat transfer and pressure distributions were generally in good agreement with experimental measurements for both attached and separated interaction regions in a Mach 10 airflow.

A series of calculations was made using the present method to study the variation in pressure, heat transfer and skin friction distributions as the strength of the adverse pressure gradient causing the interaction was varied. The change in form of the theoretical pressure distribution as the strength of the interaction increases is very similar to that observed in many experiments: a uniform pressure rise across the interaction characterizes the attached flow on a weak interaction region, while separated regions induced by strong interactions exhibit the characteristic constant pressure (plateau) region in the neighborhood of shock impingement. The predicted change in the form of the heat transfer and skin friction distributions from a cusp-like profile in an attached flow to a rounded concave form in a separated flow has been observed in experimental studies.

The final application of the present theory has been to study conditions under which a flow will just separate, i.e., incipient separation. This has been the object of many experimental studies. Criteria for determining

incipient separation in previous experimental studies have been based on changes in the form of the skin friction, pressure, and heat transfer distributions as the strength of the interaction was increased. These criteria, previously based only on experiment, are strongly supported by the calculations described in the present paper. This calculation predicted that a shock generator angle of 3.95° would cause incipient separation. This value is in excellent agreement with the experimental value of 4.2°.

The generally good agreement with experiment of the predictions from the present theory is very encouraging. However, the full range of the validity of the analysis can only be assessed by further comparison with experiment. Accordingly, the study is being continued with this objective.

REFERENCES

1. Pohlhausen, K., See page 238 et seq., "Boundary Layer Theory," Fourth Edition by Schlichting

2. Savage, S. B., The Effect of Heat Transfer on Separation of Laminar Compressible Boundary Layers, GALCIT Separated Flow Research Project Rept. No. 2 (1962)

3. Gadd, G. E., Bray, K. N. C., and Woodger, M., Some Calculations by the Crocco-Lees and Other Methods of Interactions Between Shock Waves and Laminar Boundary Layers, Including the Effect of Heat Transfer and Suction. British ARC CP 556 (1960)

4. Crocco, L. and Lees, L., A Mixing Theory for the Interaction Between Dissipative Flows and Nearly Isentropic Streams, J. Aero. Sci., Vol. 19, No. 10, pp. 649-676 (Oct. 1952)

5. Crocco, L., Considerations on the Shock-Boundary Layer Interaction. Proceedings Conference on High-Speed Aeronautics Polytechnic Institute of Brooklyn, pp. 75-112 (January 20-22, 1955)

6. Glick, H. S., Modified Crocco-Lees Mixing Theory for Supersonic Separated and Reattaching Flows. J. Aero. Sci., Vol. 29, No. 10 pp. 1238-1244 (Oct. 1962)

7. Tani, I., On the Approximate Solution of the Laminar Boundary Layer Equations. J. Aero. Sci., Vol. 21, No. 7, pp. 487-504 (July 1954)

8. Poots, G., A Solution of the Compressible Laminary Boundary Layer Equations with Heat Transfer and Adverse Pressure Gradient Quarterly Journal Mech. and Applied Math., Vol. 13, Pt. 1 (1960)

9. Abbott, D. E., Holt, M., and Nielsen, J. N., Investigation of Hypersonic Flow Separation and its Effect on Aerodynamic Control Characteristics, Vidya Report No. 81 (Sept. 1962)

10. Lees, L. and Reeves, B. L., Supersonic Separated and Reattaching Laminar Flows: I. General Theory and Application to Adiabatic Boundary Layer-Shock Wave Interactions, GALCIT Techn. Rept. No. 3., (Oct. 1963)

11. Cohen, C. B. and Reshotko, E., Similar Solutions for the Compressible Laminar Boundary Layer with Heat Transfer and Pressure Gradient. NACA Rept. 1293 (1956)

12.   Holden, M. S., Separated Flow Studies at Hypersonic Speeds
       Part II Two-Dimensional Wedge Separated Flow Studies, CAL
       Rept. No. AF-1285-A-13(2)

13.   Hakkinen, R. J., Greber, I., Trilling, L., and Abarbanel, S. S.,
       The Interaction of an Oblique Shock Wave with a Laminar Boundary
       Layer,   NASA Memo 2-18-59 (March 1959)

14.   Sterret, J. R. and Emery, J. C., Extension of Boundary-Layer
       Separation Criteria to a Mach 6.5 by Utilizing Flat Plates with
       Forward-Facing Steps   NASA TN D-618 (December 1960)

15.   Needham, D. A., A Heat Transfer Criterion for the Detection of
       Incipient Separation in Hypersonic Flow, AIAA Jour., Vol. 3,
       No. 4, pp. 781-83 (April 1965)

16.   Bogdonoff, S. M. and Vas, I. E., Some Experiments on Hypersonic
       Separated Flows   ARS Jour., Vol. 32, No. 10, pp. 1564-1572,
       (Oct. 1962)

17.   Miller, D. S., Hyman, R., and Childs, M. E., Mach 8 to 22
       Studies of Separation Due to Deflected Control Surfaces, AIAA
       Jour. Vol. 12 (Feb. 1964)

18.   Chapman, D. R., Kuehn, D. M., and Larson, H. K., Investigation
       of Separated Flows in Supersonic and Subsonic Streams with Emphasis
       on the Effect of Transition,   NASA TN 3879 (1957)

Table I
SINGLE-PARAMETER PROFILES

(A) ATTACHED REGION

$$
\begin{bmatrix} J \\ H \\ W \\ R \\ G \\ P \end{bmatrix} =
\begin{bmatrix}
.31913374 & .21801256 & -.026821239 & 0 & \\
.21510754 & .13836445 & -.020780975 & 0 & \\
.85224802 & .56173701 & .030792687 & 0 & \\
1.4660709 & -.86596556 & .45066193 & -.077378552 & -.905618 \times 10^{-3} \\
2.8905523 & -1.4646494 & .25974409 & 0 & 0 \\
-.222575 \times 10^{-3} & .53281434 & -.13683015 & .013830611 & .8588847 \times 10^{-3}
\end{bmatrix}
\times
\begin{bmatrix} a^0 \\ a^1 \\ a^2 \\ a^3 \\ a^4 \end{bmatrix}
$$

Column headers: $c_0 \quad c_1 \quad c_2 \quad c_3 \quad c_4$

$$
\begin{bmatrix} I \end{bmatrix} =
\begin{bmatrix} 3.9288028 & -9.3453917 & 7.5616817 \end{bmatrix}
\times
\begin{bmatrix} b^0 \\ b^1 \\ b^2 \end{bmatrix}
$$

$$
\begin{bmatrix} \partial J / \partial H \end{bmatrix} =
\begin{bmatrix} 1.58 & 0 \end{bmatrix}
\times
\begin{bmatrix} H^0 \\ H^1 \end{bmatrix}
$$

(B) SEPARATED REGION

$$
\begin{bmatrix} J \\ H \\ W \\ R \\ G \\ P \end{bmatrix} =
\begin{bmatrix}
.31939026 & -.21136312 & -.24067119 & -1.8380431 & 2.6162763 \\
.21365617 & -.16137034 & .052714814 & -2.2856757 & 2.8535817 \\
.85229997 & -.52481703 & -1.1702957 & 0 & 0 \\
1.4491873 & 2.1853119 & -6.7996350 & 25.656363 & 0 \\
2.9501882 & .93471792 & 4.6388347 & 21.381301 & 0 \\
.93132257 \times 10^{-8} & -.64628486 & -.84337553 & 0 & 0
\end{bmatrix}
\times
\begin{bmatrix} a^0 \\ a^1 \\ a^2 \\ a^3 \\ a^4 \end{bmatrix}
$$

$$
\begin{bmatrix} I \end{bmatrix} =
\begin{bmatrix} 7.1302172 & -33.154135 & 51.810646 \end{bmatrix}
\times
\begin{bmatrix} b^0 \\ b^1 \\ b^2 \end{bmatrix}
$$

$$
\begin{bmatrix} \partial J / \partial H \end{bmatrix} =
\begin{bmatrix} 1 \times (1.7923960) & 2 \times (-9.6275686) & 3 \times (79.341317) & 4 \times (-299.61763) & 5 \times (455.07085) \end{bmatrix}
\times
\begin{bmatrix} H^0 \\ H^1 \\ H^2 \\ H^3 \\ H^4 \end{bmatrix}
$$

Table II

TWO - PARAMETER PROFILES

(A) ATTACHED REGION ("a" constant)

$K_r(a)$	$c_{r,0}$	$c_{r,1}$	$c_{r,3}$	$c_{r,4}$
a = 0	+.15175471E+01	-.72172180E+01	+.11826745E+02	-.63025606E+01
.05	+.16696369E+01	-.81322603E+01	+.13969185E+02	-.80897173E+01
.10	+.18011203E+01	-.88815174E+01	+.15672985E+02	-.94931138E+01
.15	+.18716952E+01	-.91200082E+01	+.15962855E+02	-.96050417E+01
.20	+.19488165E+01	-.94261444E+01	+.16466635E+02	-.99203131E+01
.25	+.19939984E+01	-.95324715E+01	+.16589088E+02	-.10031949E+02
.30	+.21698984E+01	-.10659802E+02	+.19335803E+02	-.12352766E+02
.35	+.22083064E+01	-.10642245E+02	+.18939722E+02	-.11843333E+02
.40	+.20648935E+01	-.90958258E+01	+.14316718E+02	-.75081331E+01
.45	+.18054482E+01	-.65910424E+01	+.70862576E+01	-.84328705E+00
.50	+.15990186E+01	-.45597938E+01	+.12212479E+01	+.45449936E+01
.55	+.16203220E+01	-.44696962E+01	+.77783662E+00	+.49914297E+01
.60	+.19621929E+01	-.70348662E+01	+.75104608E+01	-.86050099E+00
.65	+.23251430E+01	-.99241737E+01	+.15584594E+02	-.83897254E+01
.70	+.24617465E+01	-.10830794E+02	+.17942552E+02	-.10509071E+02
.75	+.25984065E+01	-.11760926E+02	+.20394647E+02	-.12724983E+02
.80	+.26562766E+01	-.12016264E+02	+.20952415E+02	-.13201778E+02
.85	+.25907338E+01	-.11264943E+02	+.18796442E+02	-.11269470E+02
.90	+.24993300E+01	-.10287924E+02	+.16001762E+02	-.87533766E+01
.95	+.24790360E+01	-.99235414E+01	+.14914212E+02	-.77746318E+01
1.00	+.24997877E+01	-.99011868E+01	+.14745981E+02	-.75962584E+01
1.05	+.24397051E+01	-.92338813E+01	+.12894905E+02	-.59789571E+01
1.10	+.24348323E+01	-.90152416E+01	+.12229457E+02	-.53838662E+01
1.15	+.23759350E+01	-.83605456E+01	+.10409354E+02	-.37820618E+01
1.20	+.23420011E+01	-.79167962E+01	+.91739380E+01	-.27174472E+01
1.25	+.22532558E+01	-.70269050E+01	+.67348260E+01	-.57869178E+00
1.30	+.21656435E+01	-.61468370E+01	+.43280488E+01	+.15302640E+01
1.35	+.20549449E+01	-.50863213E+01	+.14476340E+01	+.40511874E+01
1.40	+.19282681E+01	-.38776961E+01	-.18729788E+01	+.69940294E+01
1.45	+.18039956E+01	-.27079733E+01	-.50657637E+01	+.98107469E+01
1.50	+.16958692E+01	-.16956462E+01	-.78009611E+01	+.12209048E+02
1.55	+.15644677E+01	-.52068895E+00	-.10919449E+02	+.14907522E+02
1.60	+.14622544E+01	+.42663687E+00	-.13484303E+02	+.17176542E+02
1.65	+.19393045E+01	-.36441714E+01	-.19342606E+01	+.66148335E+01

The leftmost bracketed column multiplies a column vector $\begin{bmatrix} b^0 \\ b^1 \\ b^2 \\ b^3 \end{bmatrix}$:

$$\left[\frac{\partial K_r}{\partial b}\right]_{b=r} = \begin{bmatrix} 1 \times c_{r,1} & 2 \times c_{r,2} & 3 \times c_{r,3} \end{bmatrix} \times \begin{bmatrix} b^0 \\ b^1 \\ b^2 \end{bmatrix}$$

45

Table II

TWO-PARAMETER PROFILES (Cont.)

(C) SEPARATED REGION ("a" constant)

$$
\begin{array}{c} K_r(a) \end{array}
\begin{bmatrix} a = 0 \\ .1 \\ .2 \\ .3 \\ .4 \\ .5 \end{bmatrix}
=
\begin{array}{ccc} c_{r.0} & c_{r.1} & c_{r.2} \end{array}
\begin{bmatrix}
2.5503995 & -14.317280 & 22.271415 \\
2.5391993 & -15.397563 & 25.328549 \\
2.4064996 & -15.623209 & 26.849987 \\
2.0800995 & -14.434495 & 25.835702 \\
1.3519996 & -9.4464247 & 16.385704 \\
0.2610205 & -3.4695036 & 7.6564012
\end{bmatrix}
\times
\begin{bmatrix} b^0 \\ b^1 \\ b^2 \end{bmatrix}
$$

$$
K_r/\ b \Big|_{b = r} = \begin{bmatrix} 1 \times c_{r.1} & 2 \times c_{r.2} \end{bmatrix} \times \begin{bmatrix} b^0 \\ b^1 \end{bmatrix}
$$

(D) SEPARATED REGION ("b" being constant)

$$
\begin{array}{c} K_r(b) \end{array}
\begin{bmatrix} b = .05 \\ .10 \\ .15 \\ .20 \\ .25 \\ .30 \end{bmatrix}
=
\begin{array}{ccc} d_{r.0} & d_{r.1} & d_{r.2} \end{array}
\begin{bmatrix}
1.8855079 & 1.0346549 & -9.2150345 \\
1.35999 & -.1167005 & -5.1859716 \\
.905 & -.69196132 & -2.5374424 \\
.5799999 & -.88995103 & -1.0323631 \\
.360 & -.72195912 & -.53396865 \\
.258 & -.57601205 & -.25203886
\end{bmatrix}
\times
\begin{bmatrix} a^0 \\ a^1 \\ a^2 \end{bmatrix}
$$

$$
\begin{bmatrix} \partial K_r / \partial\ a \end{bmatrix}_{a = r} = \begin{bmatrix} 1 \times d_{r.1} & 2 \times d_{r.2} \end{bmatrix} \times \begin{bmatrix} a^0 \\ a^1 \end{bmatrix}
$$

Table II

TWO - PARAMETER PROFILES (Cont.)

(B) ATTACHED REGION ("b" being constant)

$K_r(b)$	$d_{r,0}$	$d_{r,1}$	$d_{r,2}$	$d_{r,3}$
b =.10	.95431848	-.8065786	.1431387	-.28749421
.11	.89935031	.79684878	.10766716	-.25394235
.12	.84677488	.78579783	.0755965509	-.22308809
.13	.79653097	.77354711	.047810253	-.19480283
.14	.74356360	.76018156	.023026597	-.16897598
.15	.70281684	.74578228	.0014509857	-.14550271
.16	.6592394	.73040806	-.017053265	-.12428721
.17	.61776993	.7141821	-.032712869	-.10519953
.18	.57835864	.69714813	-.045640344	-.088153888
.19	.54094828	.67940217	-.056024009	-.07303501
.20	.50548176	.66104062	-.064053345	-.059727057
.21	.47190771	.64211816	-.069856991	-.048137887
.22	.44016622	.62274829	-.07364729	-.03814322
.23	.4102065	.60298268	-.075549202	-.029652202
.24	.38196936	.58293097	-.075770084	-.022542356
.25	.35540191	.56265996	-.074457266	-.01673999
.26	.33044973	.54224405	-.071766414	-.012064866
.27	.30705351	.52179466	-.067908392	-.0084709092
.28	.28531168	.50621736	-.07403151	-.00028325382
.29	.26529289	.47772286	-.050923195	-.0065847228
.30	.24610467	.45806257	-.047896495	-.0039648282
.31	.2279888	.44063393	-.041721453	-.0040818722
.32	.21205355	.4178829	-.031589646	-.0051593696
.33	.19464628	.4075315	-.033364909	-.0025968434
.34	.18181475	.38531394	-.020497446	-.0055090511
.35	.16959988	.37099802	-.023472516	-.0013643461
.36	.15800381	.34403285	+.0013698642	-.010019273
.37	.1470281	.33465214	-.0090670947	-.0023117469
.38	.13553251	.32646906	-.013445932	+.00062524375
.39	.12812225	.30281399	+.008219237	-.0078428003
.40	.11983134	.28201795	+.02571833	-.01404245
.41	.11315142	.26791864	+.0303865	-.015100312
.42	.10603855	.26037654	+.027673312	-.013463867
.43	.099508598	.25330465	+.024452697	-.011677842
.44	.093757623	.25013257	+.011933836	-.0052306838
.45	.087635922	.25544912	-.013649919	+.0070559056
.46	.084134592	.2419774	-.0061460123	+.0058837109
.47	.081851471	.22329308	+.0054985168	+.0050190837
.48	.077832328	.2265103	-.010035929	+.011568039

The above equals the matrix product with column vector $\begin{bmatrix} a^0 \\ a^1 \\ a^2 \\ a^3 \end{bmatrix}$

$$\left[\partial K_r / \partial a \right]_{a=r} = \left[1 \times d_{r,1} \quad 2 \times d_{r,2} \quad 3 \times d_{r,3} \right] \times \begin{bmatrix} a^0 \\ a^1 \\ a^2 \end{bmatrix}$$
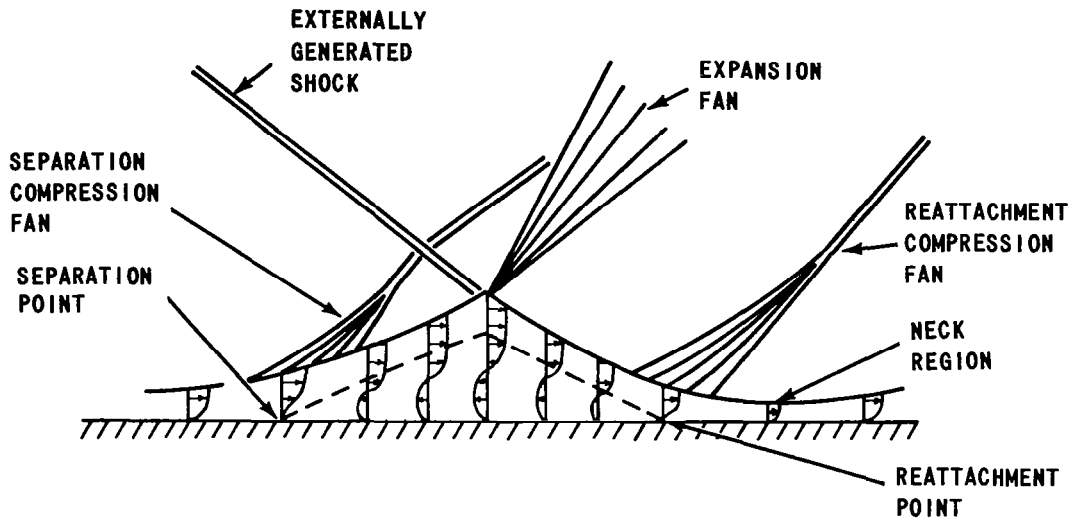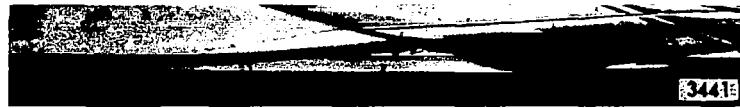
47

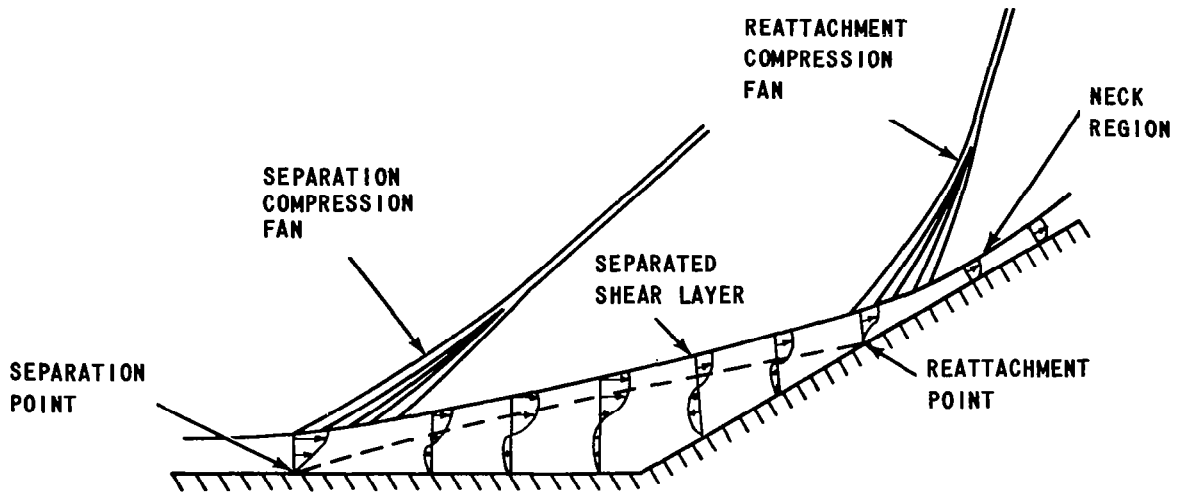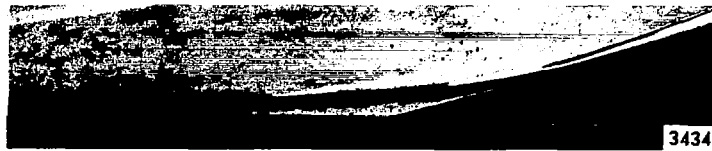Figure 1   EXTERNALLY GENERATED SHOCK-INDUCED SEPARATED FLOW

Figure 2   WEDGE-INDUCED SEPARATED FLOW

48

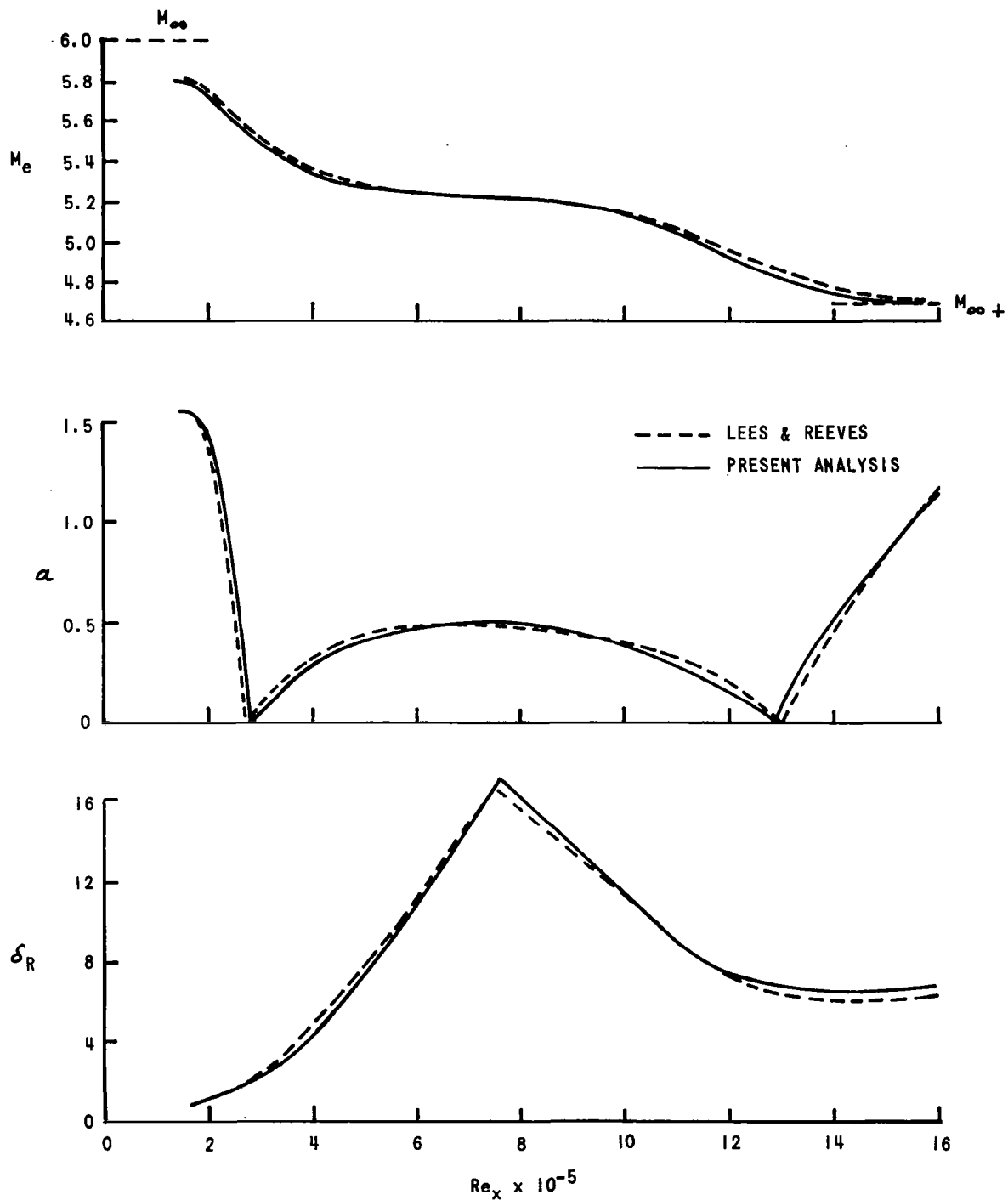Figure 3   A COMPARISON BETWEEN THE CALCULATED VALUES OF $\delta_R{}^*$, a AND M_e FOR A SHOCK WAVE – BOUNDARY INTERACTION AT M = 6, Re_{xo} = 1.7 x 10^5 OVER AN ADIABATIC WALL
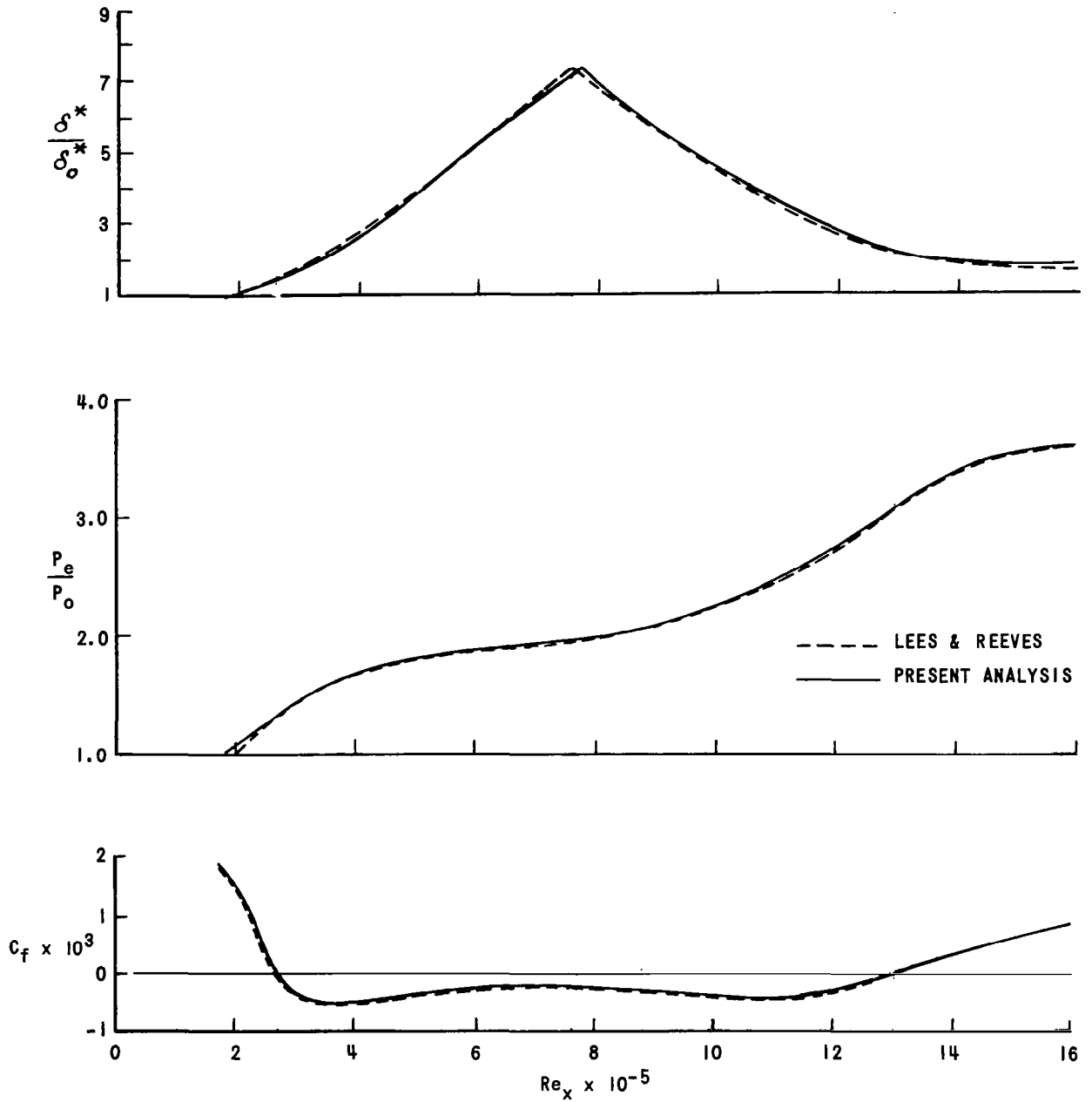
Figure 4   SHOCK WAVE - BOUNDARY LAYER INTERACTION (M = 6; Re_{xo} = 1.7 x 10^5; S_w = 0) COMPARISON BETWEEN THE PRESSURE, SKIN FRICTION AND DISPLACEMENT THICKNESS DISTRIBUTIONS
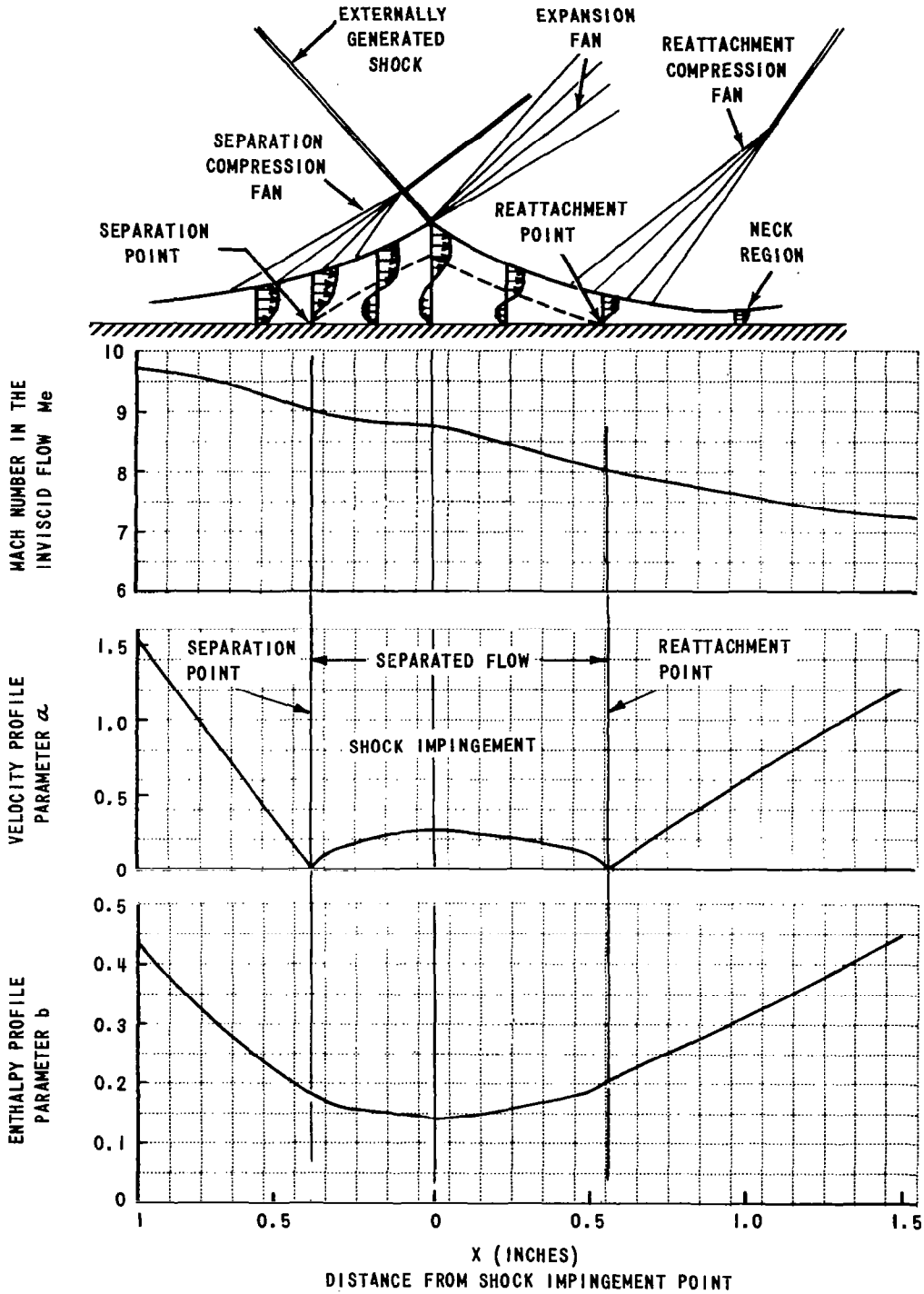
Figure 5 DISTRIBUTION OF THE PROFILE PARAMETERS AND MACH NUMBER IN THE INTERACTION REGION OF A HIGHLY COOLED SEPARATED FLOW (S_w = -0.8, M_∞ = 10; Re_x = 1.35 x 10^5/IN - ANGLE OF SHOCK GENERATOR = 5.2°).
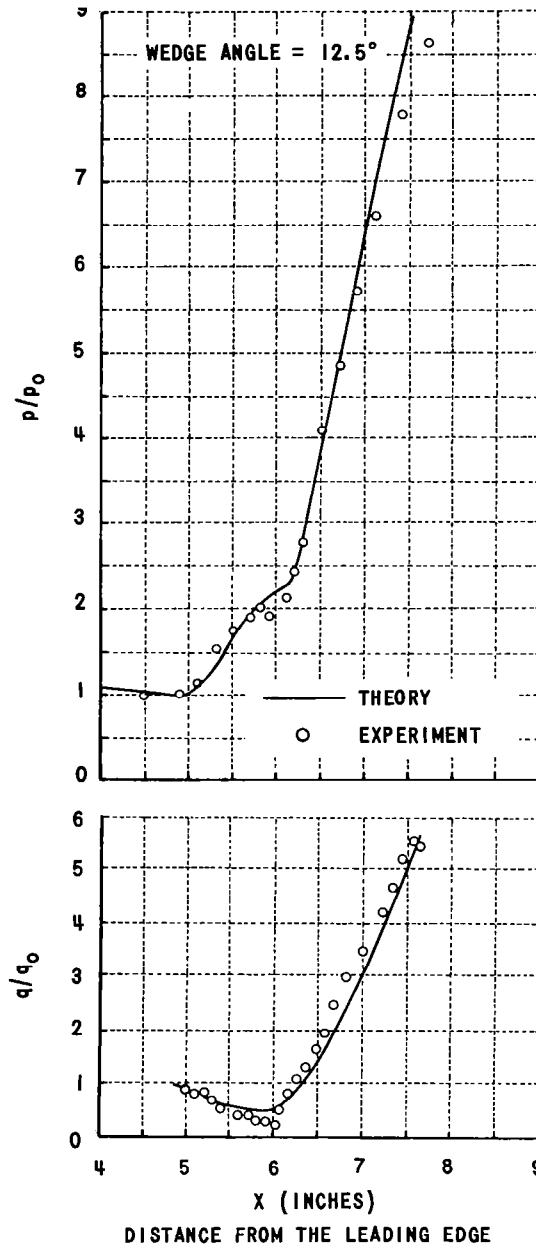
Figure 8 PRESSURE AND HEAT TRANSFER DISTRIBUTIONS IN A HIGHLY
COOLED SHOCK-INDUCED SEPARATED FLOW (S_w = -0.8, M_∞= 10;
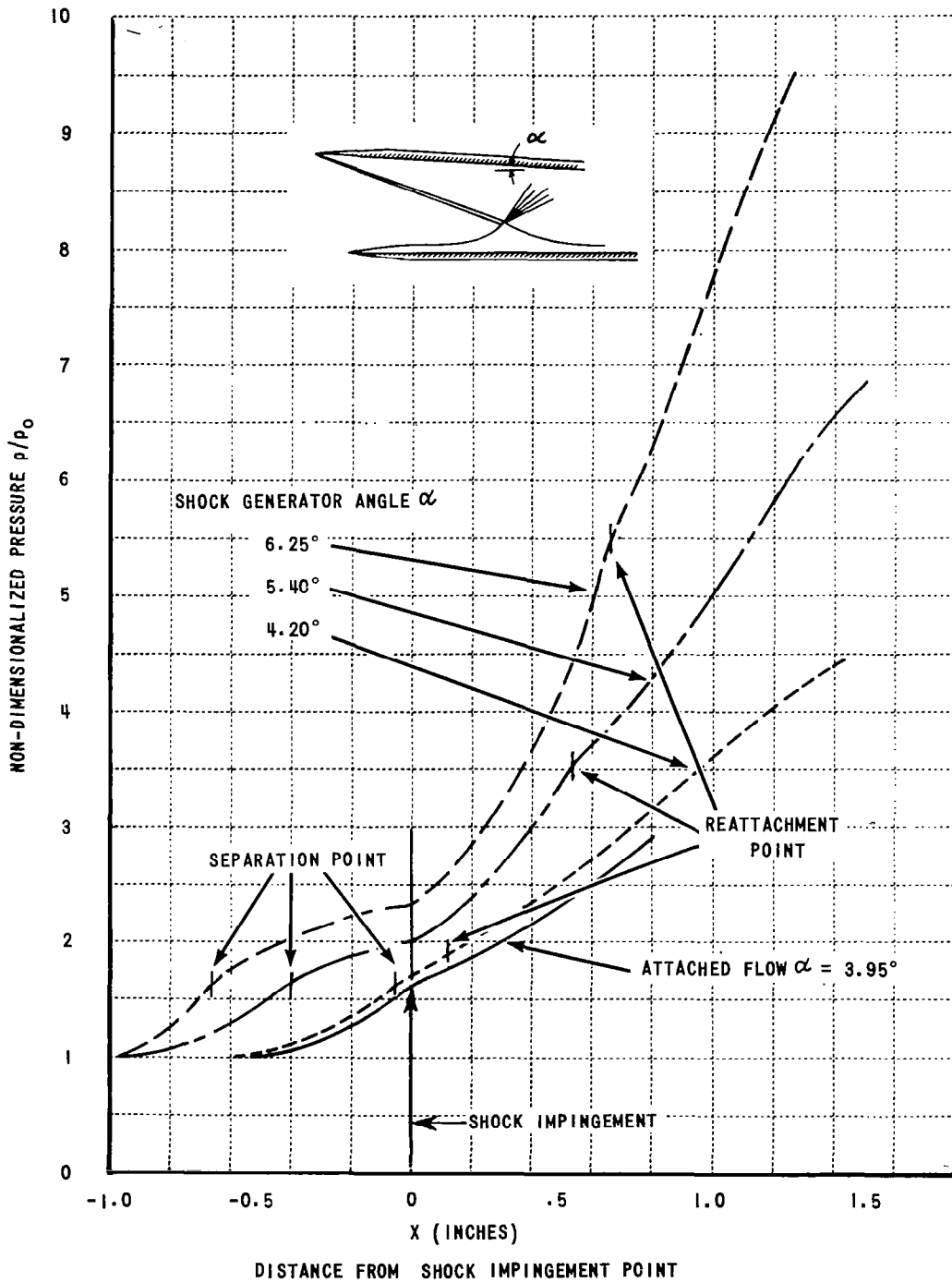Re_x = 1.35 x 10^5/IN, WEDGE ANGLE = 12.5°).

Figure 9a THE VARIATION OF THE PRESSURE DISTRIBUTION IN THE INTERACTION REGION
AS THE STRENGTH OF THE INTERACTION IS VARIED (S_W = -0.8, M_∞ = 10;
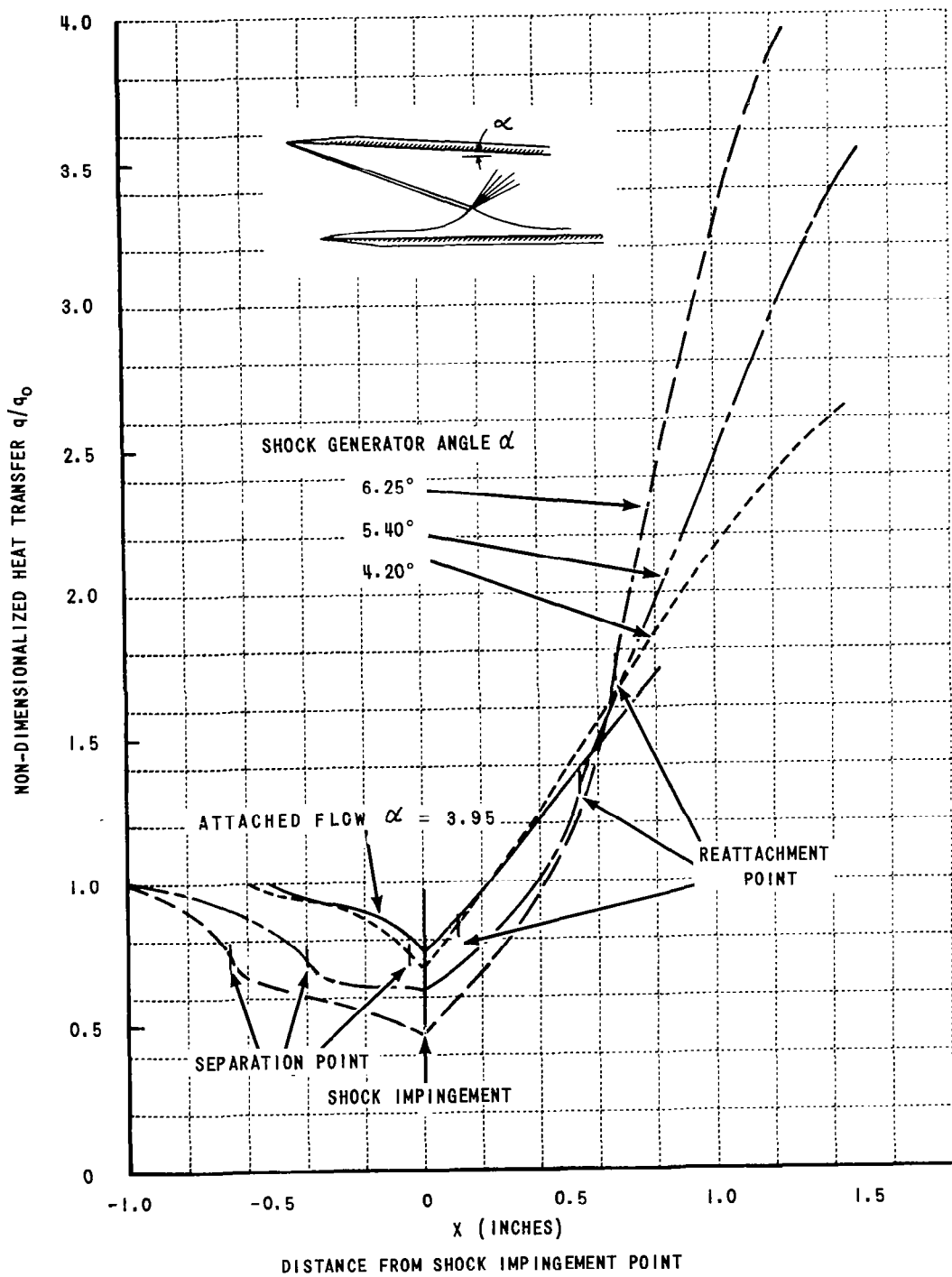Re_x = 1.35 x 10^5/IN)

Figure 9b THE VARIATION OF THE HEAT TRANSFER DISTRIBUTION IN THE INTERACTION REGION AS THE STRENGTH OF THE INTERACTION IS VARIED (S_w = -0.8, M_∞ = 10; Re_x = 1.35 x 10^5/IN)
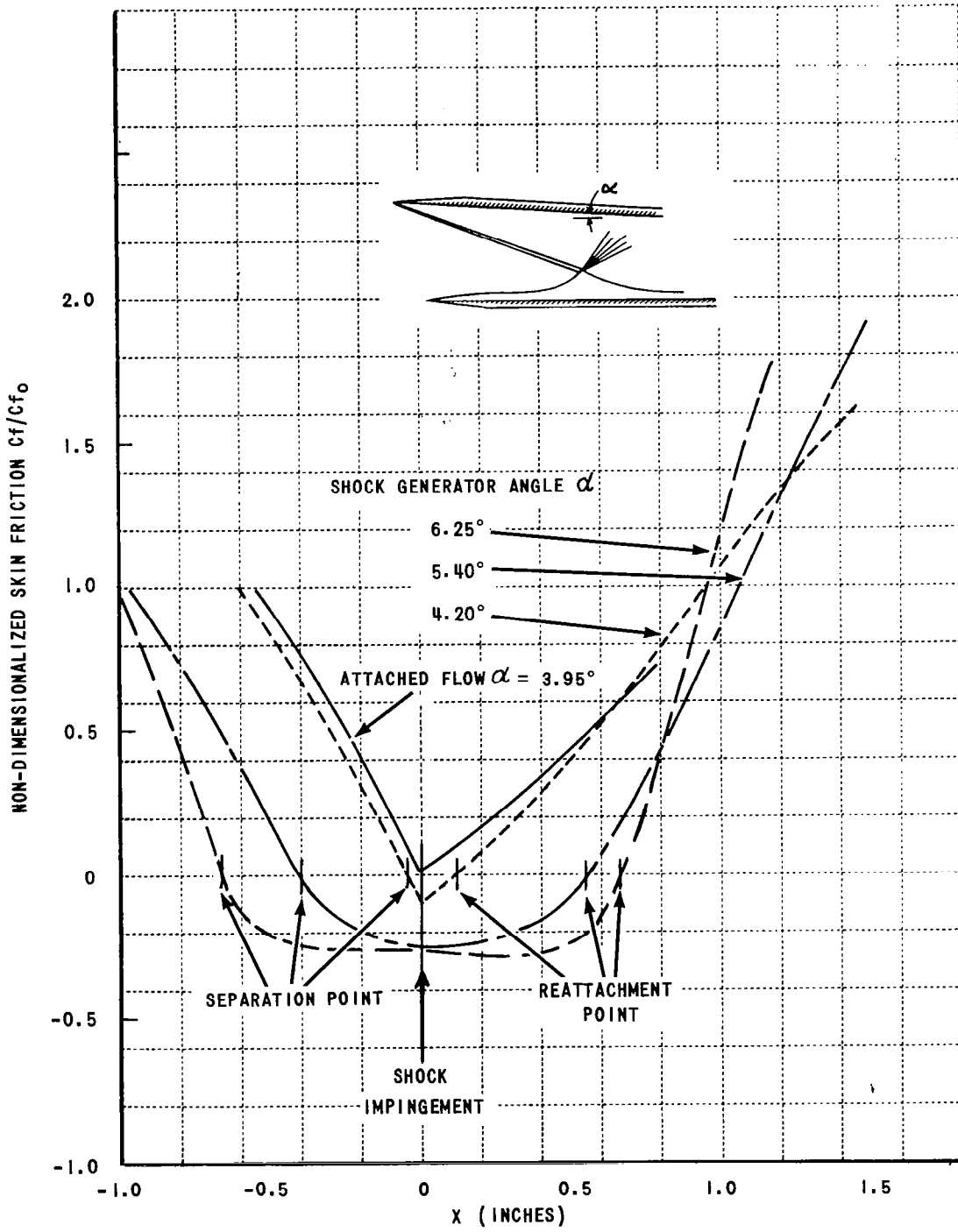
Figure 9c VARIATION OF THE SKIN FRICTION DISTRIBUTION IN THE INTERACTION REGION AS THE STRENGTH OF THE INTERACTION IS VARIED ($S_W = -0.8$, $M_\infty = 10$; $Re_x = 1.35 \times 10^5/IN$)

LINES FAIRED THROUGH EXPERIMENTAL DATA

NON-DIMENSIONALIZED HEAT TRANSFER $q/q_{FLAT\ PLATE}$

SHOCK ANGLE α	SYM
2.1	○
3.2	△
5.2	□
8.3	⬦
10.4	◇

2
1.8
1.6
1.4
1.2
1.0
.8
.6
.4
.2
4   5   6   7

DISTANCE FROM LEADING EDGE (INCHES)

(a) EXTERNALLY GENERATED SHOCK-INDUCED SEPARATION

NON-DIMENSIONALIZED HEAT TRANSFER $q/q_{FLAT\ PLATE}$

WEDGE ANGLE α	SYM
5°	⬦
7.5°	□
10°	△
12.5°	○
15°	◇

2.0
1.8
1.6
1.4
1.2
1.0
0.8
0.6
0.4
0.2
5   6   7

LINES FAIRED THROUGH EXPERIMENTAL DATA

DISTANCE FROM LEADING EDGE (INCHES)
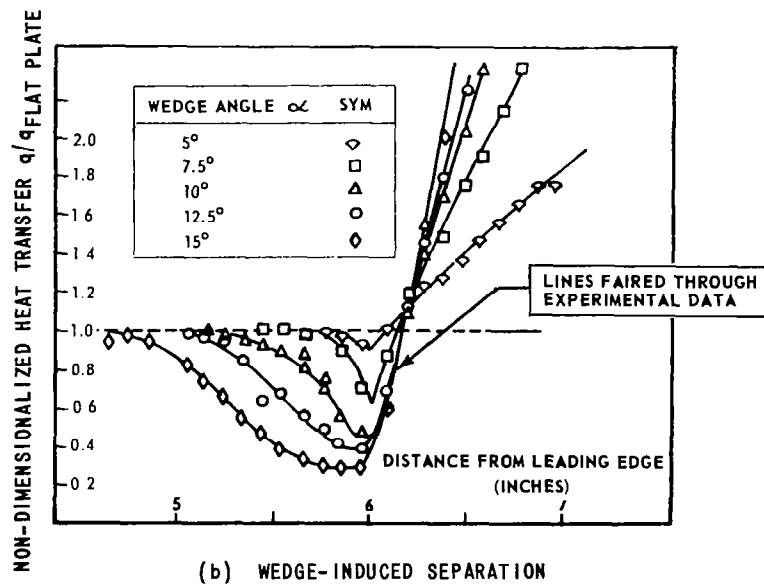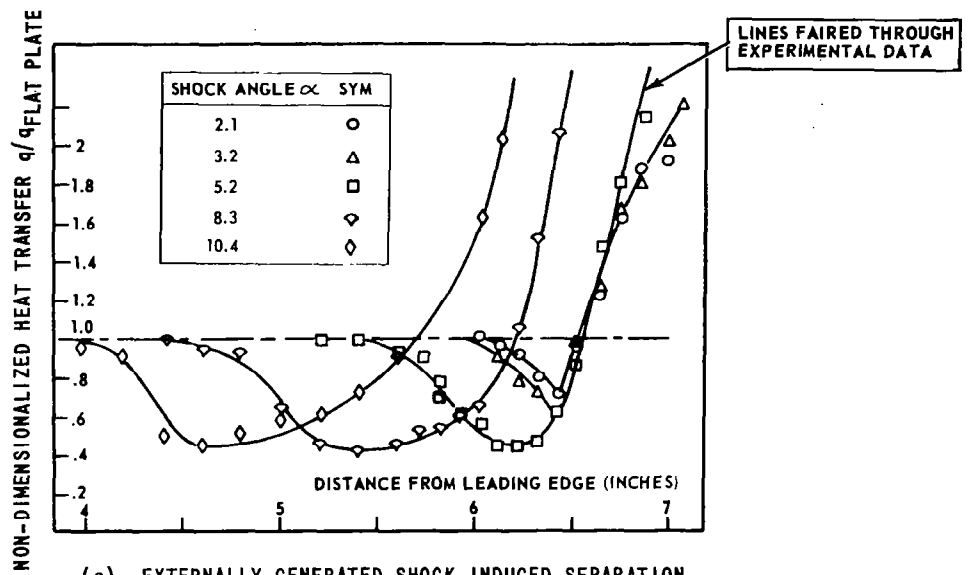
(b) WEDGE-INDUCED SEPARATION

Figure 10 EXPERIMENTAL VARIATION OF HEAT TRANSFER DISTRIBUTION IN THE INTERACTION REGION AS THE STRENGTH OF THE INTERACTION IS VARIED ($S_w = -0.8$, $M_\infty = 10$ $Re_x = 1.35 \times 10^5/IN$).